論文題目

Studies on the mechanisms of shoot-mediated control of root nodule symbiosis in *Lotus japonicus*

（ミヤコグサにおける根粒共生の地上部を介した制御機構に関する研究）

Okuma, Nao

大熊 直生

The Graduate University for Advanced Studies, SOKENDAI

School of Life Science

Department of Basic Biology

March 2021

Table of contents

Chapter 1

"General introduction"

The impact of synthetic nitrogen fertilizer on human society and the environment

Soil nitrogen is one of the most limiting factors of land plant growth and crop productivity (Oldroyd and Leyser, 2020). The invention of the industrial nitrogen fixation of atmospheric N_2 to ammonia by the Haber-Bosch process, therefore, has revolutionized the agricultural and food production system. The stable supply of synthetic nitrogen fertilizer has drastically improved crop yield per unit area of cropland, allowing a greater human population. The magnitude of the impact of the Haber-Bosch process on humanity can be seen from the estimate that about 50% of the human population is nourished by crops cultivated with synthetic nitrogen fertilizer (Erisman et al., 2008). Meanwhile, it is estimated that the world's population will increase from 7.3 billion in 2015 to 9.7 billion by 2050 (Ohyama, 2017). This means that even greater amounts of nitrogen fertilizer will need to be applied to agricultural fields to meet the increasing demand for food production due to the ever-growing population globally. However, excessive nitrogen fertilizer application is causing serious environmental pollution. For instance, about 50% of the nitrogen fertilizer applied to agricultural field is run off without being used for crops, and the leaked nitrogen fertilizer is a source of environmental pollution, such as the eutrophication of freshwater, nitrate contamination in drinking water, and rise of N_2O, a type of greenhouse gas, in the atmosphere (Zhang et al., 2015). In addition, the Haber-Bosch process mediated nitrogen fixation requires huge amounts of fossil fuels (consuming 1–2% of annual global energy consumption and about 80% of the fixed nitrogen used as nitrogen fertilizer), and causes a rise in carbon dioxide and other greenhouse gases in the atmosphere (Chen et al., 2018; Ohyama, 2017). Therefore, alternative nitrogen management is needed to reduce heavy reliance on synthetic nitrogen fertilizers without compromising crop productivity.

Nitrogen-fixing legume-*Rhizobium* symbiosis: Their great potential as an alternative nitrogen source

Effective utilization of biological nitrogen fixation by legume-*Rhizobium* symbiosis can be one of the possible ways to reduce the fertilization with nitrogen. Leguminous plants have evolved the ability to form the symbiotic interactions with soil nitrogen-fixing bacteria, collectively called rhizobia. In this symbiosis, rhizobia fix atmospheric N_2 via its bacterial nitrogenase activity and supply the host plant with ammonium. It is estimated that 21 million

tons of nitrogen are annually fixed by crop legumes through symbiosis with rhizobia (Herridge et al., 2008). Considering that the annual consumption of nitrogen fertilizer was 105 million tons in 2016 (Food and Agriculture Organization of the United Nations, 2019), biological nitrogen fixation by crop legumes has a crucial agricultural role as a source of nitrogen input to fields and has great potential to promote the reduction of nitrogen fertilizer consumption. However, it is well known that under nitrogen-replete soil (as in agricultural fields), legumes cease nitrogen fixation, because they preferentially take up and utilize soil nitrogen sources (Ledgard et al., 1996; Vinther, 1998). Therefore, to improve the utilization of the benefits of nitrogen-fixing symbiosis in agricultural fields, it is necessary to apply nitrogen fertilizer to the extent that does not limit both nitrogen fixation and legume production. It is known that the regulation of legume-*Rhizobium* symbiosis in response to inorganic nitrogen is a host plant-driven mechanism. I will briefly summarize how legumes optimize the symbiosis in the next paragraphs.

Optimization of legume-*Rhizobium* symbiosis by shoot-mediated signal transduction (autoregulation of nodulation; AON)

The symbiotic interaction between legumes and rhizobia is achieved by the formation of the host postembryonic root organ, called the nodule (Caetano-Anollés and Gresshoff, 1991; Suzaki et al., 2015). Rhizobia inhabit nodules and fix N_2 to ammonium ions. In return, the host plant supplies rhizobia with photosynthate as an energy source for nitrogen fixation. This symbiotic relationship makes it possible for legumes to utilize atmospheric N_2 and survive the nitrogen-limiting conditions. On the other hand, the cost of photosynthate for nitrogen fixation in nodules is very high. Thus, host plants need to balance the benefits of provided nitrogen nutrition from rhizobia and the cost of carbon sources for nodulation. As one of the important strategies for this, the host plant has a mechanism called autoregulation of nodulation (AON) to control nodule numbers in conditions where rhizobia have already been sufficiently infected or there are ample amounts of available nitrate in the soil. The mutants that form excessive nodules (hypernodulation) due to a defect in AON are strongly impaired in their growth. In addition, these mutants cannot cease nodulation in nitrate-sufficient conditions and impair plant growth (Nishida et al., 2018). Thus, AON is considered to have a significant functional importance in maintaining the balance between acquired nitrogen and the cost as the carbon sources for rhizobia. Therefore, understanding the molecular mechanism of AON could provide important insight such as genetic markers that help selection of superior varieties of crop legumes that can maintain their productivity with low

nitrogen fertilizer input and aid agricultural sustainability. Here, I will summarize the current model of AON.

Molecular basis of AON

AON is achieved by signal transduction between roots and the shoot through a shoot-acting leucine-rich repeat receptor-like kinase (LRR-RLK). The LRR-RLK was isolated from hypernodulation mutants of various legume species (Caetano-Anollés and Gresshoff, 1991; Reid et al., 2011b), and designated HYPERNODULATION ABERRANT ROOT1 (HAR1) in *Lotus japonicus* (Krusell et al., 2002; Nishimura et al., 2002; Wopereis et al., 2000), SUPER NUMERIC NODULES (SUNN) in *Medicago truncatula* (Schnabel et al., 2005), NODULE AUTOREGULATION RECEPTOR KINASE in soybean (Searle et al., 2003), and SYM29 in pea (Krusell et al., 2002). Reciprocal grafting of these mutants demonstrated that these LRR-RLKs act in the shoot systemically to inhibit nodule formation in the roots. These LRR-RLKs have an indispensable role in AON to perceive root-derived mobile CLV3/ESR-related (CLE) peptides such as CLE ROOT SIGNAL 1, 2, and 3 (CLE-RS1, 2, and 3) in *L. japonicus* (Nishida et al., 2016; Okamoto et al., 2009, 2013a), CLE12 and CLE13 in *M. trunctula* (Mortier et al., 2010), and RHIZOBIA-INDUCED CLE1 (RIC1) and RIC2 in soybean (Reid et al., 2013, 2011a). All of these peptides are synthesized in roots in response to rhizobial infection or high soil nitrate concentrations. In *L. japonicus*, tri-arabinosylation of CLE-RS2 peptide is required for the direct binding of HAR1 and suppression of nodulation in a HAR1-dependent manner (Okamoto et al., 2013a). Moreover, the inhibitory effects of CLE peptides on nodulation in *L. japonicus* depend partially on the gene known as *PLENTY*, which encodes hydroxyproline-*O*-arabinosyl transferase (HPAT) (Yoro et al., 2019). In *M. truncatula*, mutants of *ROOT DETERMINED NODULATION1* (Kassaw et al., 2017; Schnabel et al., 2011), an orthologous gene to *PLENTY,* show a similar phenotype to *plenty*. Thus, arabinosylation of CLE peptides by HPATs is likely to be required for them to be recognized by LRR-RLKs. After CLE peptides are perceived by the shoot-acting LRR-RLK, nodulation in roots becomes inhibited by TOO MUCH LOVE (TML), the gene for which was isolated from hypernodulation mutants of *L. japonicus* (Magori et al., 2009; Takahara et al., 2013). Since *TML* encodes an F-box/kelch repeat protein, it is hypothesized that TML may be involved in ubiquitin proteasome-mediated degradation of unknown target proteins that are associated with early nodule development (Takahara et al., 2013). *M. truncatula* has two *TML* orthologues, *TML1* and *TML2*, which inhibit nodule formation downstream of

SUNN (Gautrat et al., 2019). Hence, these factors that are involved in systemic signaling are well-conserved in legume species.

Shoot-root signaling communication: A crucial adaptation strategy of plants to environmental fluctuation

The long-distance signaling system is widely adopted in land plants to adapt to various environmental changes. For example, information on light conditions for the leaves (Chen et al., 2016) and nitrogen deficiency in the roots (Tabata et al., 2014), is transferred using a long-distance communication system (Ko and Helariutta, 2017). Shoot-root communications are accomplished delivering signaling molecules between the shoot and roots, such as proteins (Chen et al., 2016), peptides (Ohkubo et al., 2017; Okamoto et al., 2013a; Ota et al., 2020; Tabata et al., 2014), phytohormones (Landrein et al., 2018; Poitout et al., 2018; Sasaki et al., 2014), and RNA species (Banerjee et al., 2009; Lin et al., 2008; Tsikou et al., 2018) in response to various environmental cues. These systemic signalings are crucial for land plants to thrive under fluctuating environments. I will describe the importance of these systemic signaling with the following two examples.

Since light status has a significant impact on the growth and development at the whole plant level, the light status perceived in the shoots must be promptly transmitted to roots to coordinate the developmental and physiological processes both in the shoot and roots. In *Arabidopsis thaliana* (hereafter, Arabidopsis), ELONGATED HYPOCOTYL5 (HY5) protein, a bZIP transcription factor, is a shoot-to-root mobile signal that is required to facilitate light-activated, physiological adaptation and growth promotion of roots (Chen et al., 2016). Grafting experiments of *hy5* mutant and WT demonstrate that shoot-derived HY5 systemically regulates root growth and nitrate uptake through activation of nitrate transporter NRT2.1 in a light-dependent manner. In addition, HY5 in the shoots enhances carbon assimilation and transport of sugar to roots through activation of its target gene in response to light. Since the carbon/nitrogen (C/N) ratio of the *hy5* mutant is increased in a light intensity-dependent manner, where wild-type is stable, shoot-derived HY5 is necessary to coordinate C/N balance under fluctuating light conditions.

In natural environments, soil nitrate is heterogeneously distributed. To adapt to such a fluctuating nitrate environment, land plants sense local nitrate availability in each root and share this information through root-shoot-root long-distance signaling. In Arabidopsis, the small peptide hormone C-TERMINALLY ENCODED PEPTIDE (CEP) is adopted as a long-distance signal that informs local soil nitrate deficiency on one side of roots to distant roots

(where nitrate availability is relatively high), through root-derived CEP recognition by the shoot-localized LRR-RK, CEP receptor 1 (CEPR1), and CEPR2 (Ohkubo et al., 2017; Tabata et al., 2014). After perception of CEP by CEPR1 and CEPR2, CEP DOWNSTREAM 1 (CEPD1) and CEPD2 are induced and synthesized in the shoot. CEPD1 and CEPD2 are translocated from the shoot to the roots and enhance nitrate uptake through activation of *NRT2.1*. *cepd1/2* and *cepr1* mutants cannot induce *NRT2.1* under nitrate deficit conditions and produce pale green leaves, a symptom of nitrogen deficiency, thereby CEP-mediated root-shoot-root signaling transduction is necessary to maintain nitrate homeostasis in heterogeneous nitrate conditions.

Summary and objectives of this dissertation

As mentioned above, the nitrogen fixation of legume-*Rhizobium* symbiosis can contribute to achieving sustainable agriculture by reducing nitrogen fertilizer usage. On the other hand, especially in agricultural fields where there is sufficient nitrogen, the benefit of this symbiosis cannot be maximized because legumes stop nodule formation via AON. Since AON is thought to be a mechanism for optimizing the number of nodules under fluctuating environments, understanding the molecular mechanism of AON provides important knowledge that could contribute to breeding crop legumes that can be cultivated with reduced nitrogen fertilizer without compromising their productivity. In addition, since the shoot-root long-distance signaling systems are widespread adaptation strategies against nutrient deficiencies in land plants, the molecular basis of AON could provide insights into how plants inform nutritional fluctuation through shoot-root communication. In this dissertation, I attempted to expand our knowledge of AON, as shown in Chapters 2 and 3 below (Fig. 1.1).

In Chapter 2, I attempted to reveal the detailed molecular mechanism of shoot-mediated, long-distance regulation of nodulation in AON. In *L. japonicus*, shoot-to-root transfer of microRNA miR2111 that targets mRNA of *TML* has been proposed to explain the mechanisms underlying nodulation control from the shoot. However, it is still controversial as to whether or not shoot-derived miR2111s can regulate nodulation and *TML* mRNA levels in roots. Also, which miR2111 genes are responsible for AON is unknown. Therefore, I focused on miR2111 to clarify the detailed regulatory mechanism of nodulation from the shoot (Fig. 1.1).

In Chapter 3, I focused on the potentially overlooked role of HAR1 in shoots, which is distinct from the control of nodulation. In the current model, it is not clear why AON signaling acts via the shoot-acting HAR1 receptor, because both the first and last events of

AON (the response to rhizobial/nitrate and the inhibition of nodulation) occur in roots. Hence, I hypothesized that HAR1 may have functions in the shoot other than the regulation of nodulation in roots. Indeed, mutants of HAR1 and its orthologue in soybean exhibit smaller leaf cell numbers and leaf sizes compared to the wild-type, regardless of symbiotic or non-symbiotic conditions (Ito et al., 2008; Tanabata et al., 2013). To fully understand the implication of shoot-mediated signalling of AON, elucidation of the unknown functions of HAR1 in the shoot is necessary. Through transcriptomic analysis, I characterized genes regulated by HAR1 in leaves by *CLE-RS1*/*2* overexpression in addition to either rhizobial inoculation or nitrate treatment. In addition, I searched for phenotypic differences in *har1-7* shoots estimated from genes whose expression was induced in a HAR1-dependent manner (Fig. 1.1).

Chapter 2

"*MIR2111-5* locus and shoot-accumulated mature miR2111 systemically enhance nodulation depending on HAR1 in *Lotus japonicus*"

2.1 Introduction

To optimize the number of nodules, legumes utilize a long-distance negative feedback mechanism known as AON (Suzaki et al., 2015). Although the interaction between the root-derived signal, CLE peptides, and shoot-acting receptors, such as HAR1, is well characterized, the detailed regulatory mechanism of nodulation by shoot-derived signals is still unclear.

Two types of molecules generated in shoots downstream of shoot-acting receptors that are involved in AON have been reported to date. One is a phytohormone, cytokinin. In *L. japonicus*, cytokinin accumulates in shoots in a HAR1-dependent manner after inoculation with rhizobia (Sasaki et al., 2014). When exogenously applied to shoots, cytokinin causes a decrease in nodule numbers depending on *TML*. The other factor is miRNA miR2111, which targets *TML* mRNA and enhances nodulation (Gautrat et al., 2020; Tsikou et al., 2018). In *L. japonicus* and *M. truncatula*, the accumulation of mature miR2111s is drastically reduced in both the shoot and the roots in response to rhizobial infection and nitrate treatments, depending on *HAR1*/*SUNN*. Thus, *HAR1*/*SUNN* negatively regulates the accumulation of miR2111s to enhance nodulation under non-inoculated or nitrate-deficient conditions (Gautrat et al., 2020; Tsikou et al., 2018).

A substantial portion of miRNA gene families in plants consists of multiple loci (Kozomara and Griffiths-Jones, 2011; Li and Mao, 2007; Maher et al., 2006). Each individual locus in a certain miRNA gene family often exhibits different expression levels and patterns and sometimes is involved in distinct developmental processes even though the target genes are shared in the gene family (Carlsbecker et al., 2010; Jiang et al., 2006; Miyashima et al., 2013; Tatematsu et al., 2015). Three loci for miR2111 (*MIR2111-1, -2,* and *-3*) have been reported in *L. japonicus* (Tsikou et al., 2018). Ectopic overexpression of *MIR2111-3* in hairy roots increases the amount of mature miR2111s and nodule numbers. Because the activity of *MIR2111-3* promoter is detected predominantly in the phloem of leaves, translocation of shoot-derived mature miR2111s into roots has been proposed to explain anticorrelation between the levels of mature miR2111s and of *TML* mRNA in roots. However, it remains unclear whether or not *MIR2111-3* is a responsible locus for AON since *MIR2111-3*

expression levels and its dependency on HAR1 have not been evaluated. Moreover, systemic regulation by shoot-accumulating mature miR2111s of nodulation has not been clearly shown. In a previous study by Tsikou et al., the shoot-to-root transfer of mature miR2111s was explained by decreased mature miR2111 levels in the roots that were mechanically separated from the shoot (shoot-less roots) (Tsikou et al., 2018). Nodule numbers were also decreased in the shoot-less roots. However, these experiments need to be considered that the removal of shoots generates mechanical stresses and influences many other factors that are synthesized in and transferred from shoots photosynthate and phytohormones.

In this study, I identified four *L. japonicus* miR2111 loci, the expression of which was detected in leaves and controlled by HAR1 LRR-RLK. I attempted reverse genetic analyses such as CRISPR and short tandem target mimic (STTM) technologies to elucidate the function of highly regulated miR2111 loci on shoot-mediated control of nodulation. Furthermore, I examined whether or not shoot-derived miR2111 is sufficient for the systemic regulation of nodulation in roots by grafting experiments using miR2111 overexpressed line and down-regulated lines.

2.2 Results

Identification of *MIR2111-2*, *-4*, *-5*, and *-7*, the expression of which is repressed by rhizobial infection in a *HAR1*-dependent manner

Three genomic loci for miR2111 precursors (*MIR2111-1, -2,* and *-3*) have been reported in *L. japonicus* (Table 2.1). These miR2111 gene loci contain a total of five miR2111 hairpin sequences, which generate three mature miR2111 isoforms, miR2111a, miR2111b, and miR2111c (Tsikou et al., 2018). I investigated additional potential miR2111 hairpin sequences using BLAST search with an improved reference genome assembly for *L. japonicus* (Gifu v1.2) (Kamal et al., 2020), and hairpin structure prediction (Camacho et al., 2009; Reuter and Mathews, 2010). In addition to the five known miR2111 hairpin sequences, I identified five sequences that are potentially processed to become miR2111s and designated a total of miR2111 hairpin sequences as miR2111-A to miR2111-J (Table 2.1, Fig. 2.1a). The five new sequences were predicted to form hairpin structures containing mature miR2111 sequences in their stems (Fig. 2.1b). However, the predicted structures of three hairpin sequences (miR2111-F, -H, and -J) were not typical among reported miRNA structures since they have the miR2111 duplex at the proximal end of the hairpin structure (Mateos et al., 2010; Moro et al., 2018; Werner et al., 2010) (Fig. 2.1b).

Next, I carried out RNA-seq analyses in mature leaves of *L. japonicus* (2 weeks after germination) to examine the expression of miR2111 precursors and performed RNA-Seq-based gene prediction using Stringtie (Pertea et al., 2015) to identify functional miR2111 loci containing predicted hairpin structures (Fig. 2.2a-d), because miRNAs are generated by processing of primary transcripts of miRNA genes (pri-miRNAs), which are polycistronic in some cases. I detected four pri-miR2111 sequences and named their genes *MIR2111-2*, *MIR2111-4*, *MIR2111-5*, and *MIR2111-7* (Fig. 2.2a-d). *MIR2111-4* and *MIR2111-5* are monocistronic miR2111 loci containing miR2111-F and miR2111-G, respectively. *MIR2111-2 and MIR2111-7* are polycistronic and possess dual hairpin structure sequences. *MIR2111-2* contains the sequences for miR2111-B and miR2111-C, whereas *MIR2111-7* possesses the sequences for miR2111-I and miR2111-J (Fig. 2.1a, b; Table 2.1). The nucleotide sequence of *MIR2111-7* showed 96% identity with that of *MIR2111-2*, suggesting that these two loci are paralogous. Furthermore, I searched new potential miR2111 genes that were not detected from my RNA-seq data by BLASTn search using all miR2111 gene sequences as the query. I found a *MIR2111-4* paralogous sequence and named it *MIR2111-6*, which showed 93% identity with *MIR2111-4* and contained the sequence for miR2111-H (Fig. 2.1a).

Apart from *MIR2111-1* on chromosome 1, each monocistronic and polycistronic miR2111 locus was tandemly paired and arranged near the pericentromeric region of chromosome 3 (Fig. 2.1a, b). It is noteworthy that three of the four pri-miR2111s that were expressed in leaves, *MIR2111-4*, *MIR2111-5*, and *MIR2111-7*, were different from the known miR2111 loci. In addition, the *MIR2111-2* transcript detected in this study was much longer (789 bp) than that reported previously (312 bp) (Tsikou et al., 2018).

Expression of *MIR2111-2*, *MIR2111-4*, *MIR2111-5*, and *MIR2111-7* was repressed in wild-type (WT) leaves in response to rhizobial inoculation but not in the *har1-7* mutant (Fig. 2.2a-d), suggesting that expression of these miR2111 genes were negatively regulated by *HAR1*. *MIR2111-5* showed 3–5-fold higher transcripts per million (TPM) values than the other miR2111 genes expressed in leaves of mock-treated WT and *har1-7* (Fig. 2.2b). Expression of *MIR2111-1*, *MIR2111-3*, and *MIR2111-6* was below detectable levels in my RNA-seq data (Fig. 2.3).

MIR2111-2 and MIR2111-5 promote nodulation and mature miR2111 accumulation

I evaluated nodulation phenotypes of *L. japonicus* roots ectopically overexpressing the miR2111 genes that I identified to confirm whether or not the genes are functional. I chose *MIR2111-2*, *MIR2111-4*, and *MIR2111-5* from among the four miR2111 genes that

demonstrated expression in leaves. *MIR2111-7* was not incorporated into the functional analyses since it was over 90% identical to *MIR2111-2*. For the overexpression assay, DNA fragments fully covering pri-miRNA regions (about 700–900 bp) were expressed under an *L. japonicus Ubiquitin* promoter (*proUBQ*) (Maekawa et al., 2008) (Fig. 2.1a-d). I generated hairy roots transformed with either *proUBQ:MIR2111-2*, *proUBQ:MIR2111-4*, or *proUBQ:MIR2111-5*. Nodule numbers were counted in transformed roots displaying fluorescence of a GFP transformation marker at 21 days after inoculation (dai) with DsRed-labeled *Mesorhizobium loti*. Furthermore, I conducted qRT-PCR analyses to examine the accumulation of mature miR2111s and *TML* mRNA in transformed roots at 5 dai.

Nodule numbers were significantly increased in roots transformed with *proUBQ:MIR2111-2* and *proUBQ:MIR2111-5* compared with empty vector controls (Fig. 2.4a-e); the mean nodule numbers were about 5- and 8-fold higher in *proUBQ:MIR2111-2* and *proUBQ:MIR2111-5* roots, respectively (Fig. 2.4e). In addition, these transformed roots produced mature nodules that were seemingly smaller than those in control roots, similarly to *tml* roots (Magori et al., 2009) (Fig. 2.4a-d). *proUBQ:MIR2111-2* and *proUBQ:MIR2111-5* also increased the accumulation of mature miR2111s about 20-fold and 180-fold over controls, respectively (Fig. 2.4f). Conversely, the abundance of *TML* mRNA was decreased in these transformed roots (Fig. 2.4f). These results indicated that *MIR2111-2* and *MIR2111-5* enhanced nodulation and inhibited *TML* mRNA accumulation similarly to *MIR2111-3* (Tsikou et al., 2018). Therefore, I concluded that *MIR2111-2* and *MIR2111-5* were functional in promoting nodule formation by influencing the accumulation of *TML* mRNA.

However, *proUBQ:MIR2111-4* influenced neither the number of nodules nor *TML* mRNA accumulation, even when the levels of mature miR2111s in the transformed roots I detected by qRT-PCR were comparable with those in roots transformed with *proUBQ:MIR2111-2* (Fig. 2.4f). This result suggested that *MIR2111-4* is not functional with respect to regulating nodule numbers.

MIR2111-5 is expressed predominantly in the phloem of mature leaves in a *HAR1*-dependent manner

My RNA-seq analyses showed that, among *L. japonicus* miR2111 loci, *MIR2111-5* most abundantly accumulated in leaves of non-inoculated plants. In addition, compared with the other miR2111 loci tested, *MIR2111-5* overexpression in roots was the most effective at increasing the number of nodules. Therefore, I focused on *MIR2111-5* in further analyses.

In order to characterize the spatial expression pattern of *MIR2111-5*, a 3.0 kb DNA fragment upstream of *MIR2111-5* was inserted upstream of a GUS reporter gene. Histochemical GUS staining assay was conducted using plants stably transformed with this reporter construct (*proMIR2111-5:GUS*). GUS staining was detected along with vascular bundles in true leaves and cotyledons of two-week-old plants (Fig. 2.5a). At this point after germination, *L. japonicus* MG-20 seedlings have two sets of fully expanded leaves. GUS expression was detected strongly in the more mature leaves, while much weaker expression was seen in younger leaves (Fig. 2.5a). GUS expression tended to be clear in vascular bundles around the leaf margins and cotyledons but was not detected in midveins (Fig. 2.5a). In contrast, GUS signals were negligible in stems, roots, and root nodules (Fig. 2.6a-d). This GUS expression along with vasculatures was attenuated within 5 dai with *M. loti* (Fig. 2.5b). Cross-sections of leaves revealed that the GUS reporter was expressed mainly in the phloem (Fig. 2.5c, d), which is similar to the expression pattern previously reported for *MIR2111-3* (Tsikou et al., 2018).

Next, I examined the effects of rhizobial infection on the accumulation of mature miR2111s, *MIR2111-5*, and *TML* mRNA in leaves and roots by qRT-PCR. Mature miR2111s were clearly detected in both leaves and roots of mock controls and accumulation decreased within 3 dai in a *HAR1* dependent manner (Fig. 2.5e, f). *TML* mRNA levels were negatively correlated with the accumulation of mature miR2111s in roots (Fig. 2.5i). Similar to mature miR2111s, the abundance of *MIR2111-5* in leaves also altered in response to inoculation with *M. loti* depending on *HAR1* (Fig. 2.5g). However, the accumulation of *MIR2111-5* in roots was sustained at very low levels or below detectable levels, even in *har1-7* roots where mature miR2111s accumulated in abundance (Fig. 2.5h). Patterns of endogenous *MIR2111-5* accumulation were similar to those of GUS expression driven by its own promoter (Fig. 2.5a, b; Fig. 2.6a-d).

The accumulation of mature miR2111s in shoots is sufficient to enhance nodulation in roots

According to the current hypothesis, mature miR2111s are synthesized in leaves and translocated to roots via phloem vessels to activate nodulation through post-transcriptional inhibition of *TML* mRNA accumulation (Tsikou et al., 2018). Consistent with this hypothesis, the promoter activity of *MIR2111-5* was predominantly detected in the phloem of leaves and cotyledons (Fig. 2.5a-d). Indeed, *MIR2111-5* was abundant in leaves of uninoculated plants

(Fig. 2.5g). Nevertheless, it was unclear whether shoot-derived miR2111 truly be able to systemically enhance nodulation in roots.

To clarify the functional relevance of shoot-derived miR2111s in nodulation, I generated stable *proUBQ:MIR2111-5* transgenic lines (*MIR2111-5*ox) (Fig. 2.7). *MIR2111-5*ox displayed significantly increased nodule and infection thread numbers. Next, I performed reciprocal grafting between *MIR2111-5*ox and WT plants. Scions overexpressing *MIR2111-5* significantly increased nodule numbers in WT rootstocks (28 dai) (Fig. 2.8a-e). This result indicated that *MIR2111-5* overexpression in shoots was sufficient to promote nodulation. Next, I examined the effects of *MIR2111-5* overexpressed scions on the accumulation of mature miR2111s, *MIR2111-5*, and *TML* mRNA in rootstock using qRT-PCR. WT rootstocks grafted with *MIR2111-5*ox scions showed significant increases in mature miR2111s and a reduction of *TML* mRNA levels (5 dai) (Fig. 2.8f), indicating that *MIR2111-5* overexpression in shoots can systematically regulate the accumulation of mature miR2111s and *TML* mRNA in roots. Grafting between *MIR2111-5*ox scions and *tml-4* rootstocks or *har1-7* scions and *MIR2111-5*ox rootstocks did not exhibit additive effects on nodule numbers compared with self-grafted mutant plants, suggesting that *MIR2111-5* functioned in the same genetic pathway as *HAR1* and *TML* in the control of nodule number (Fig. 2.9).

In contrast to mature miR2111s, *MIR2111-5* levels in WT rootstocks grafted with *MIR2111-5*ox scions were very low or below detectable levels (Fig. 2.8f). To confirm whether or not shoot-derived mature miR2111s promote nodulation in roots, I designed a short tandem target mimic (STTM) construct (Yan et al., 2012) to prevent the accumulation of mature miR2111s (*proUBQ:STTM2111*) and generated stable *proUBQ:STTM2111* transgenic lines (STTM2111). In leaves of STTM2111, the abundance of mature miR2111s was reduced by less than half of that in WT plants, whereas the levels of *MIR2111-5* were not influenced, indicating that STTM2111 successfully inhibits mature miR2111s (Fig. 2.10). Next, I carried out reciprocal grafting experiments between STTM2111 and WT plants. STTM2111 scions significantly reduced nodule numbers in the WT rootstocks to those equivalent to STTM2111 rootstocks (Fig. 2.8g). Thus, the amount of mature miR2111s generated in shoots is crucial to increasing nodule numbers in the roots.

MIR2111-5 locus is required to increase root nodule numbers

Although overexpression of *MIR21111-5* significantly increased nodule numbers and mature miR2111 accumulation in roots, it remained unknown to what degree *MIR2111-5* locus contributes to producing mature miR2111s and controlling nodule numbers. To address this

issue, I generated two knockout lines of *MIR2111-5*, *mir2111-5-1* and *mir2111-5-2*, using a CRISPR technology with dual gRNA-containing constructs (Fig. 2.11a; see Methods). In *mir2111-5-1* and *mir2111-5-2*, the mature miR2111 sequence was partially or completely deleted (Fig. 2.11a).

The deletion of *MIR2111-5* significantly decreased the nodule and infection thread number compared with the WT (Fig. 2.11b). Furthermore, the abundance of mature miR2111s in these leaves and roots was reduced to less than half of that seen in the WT (Fig. 2.11c). *TML* mRNA levels were not significant but tended to be higher in roots of *mir2111-5* mutants than those of the WT (Fig. 2.11c). These results suggested that *MIR2111-5* locus is necessary to increase the amount of mature miR2111s in leaves and roots and the number of nodules in roots.

2.3 Discussion

Land plants adapt to environmental stimuli, such as soil nutrient deprivation at the whole plant level by shoot-mediated signaling communication via vascular bundles (Ko and Helariutta, 2017). In this study, I investigated the functions of miR2111 genes in the shoot-mediated nodulation control system known as AON, focusing, in particular, on *MIR2111-5* locus. *L. japonicus* possesses at least seven miR2111 genes including those I identified and four genes expressed in leaves (Fig. 2.2; Fig. 2.1a, b). Grafting experiments demonstrated that the accumulation of mature miR2111s in shoots was sufficient to increase the number of root nodules and reduce the accumulation of their targets, *TML* mRNA, in roots (Fig. 2.8). Moreover, I found that *MIR2111-5* locus, which was expressed mainly in leaves (Fig. 2.5; Fig. 2.6), was required for the regulation of nodule number and accumulation of mature miR2111s in roots (Fig. 2.11). Thus, mature miR2111s accumulation in leaves through *MIR2111-5* expression is necessary to systemically optimize nodule number in a HAR1-dependent manner.

Four miR2111 genes, *MIR2111-2*, *MIR2111-4*, *MIR2111-5*, and *MIR2111-7*, were expressed in leaves and repressed after rhizobial inoculation in a *HAR1*-dependent manner, whereas expression of the others was not detected by my RNA-seq analyses (Fig. 2.2; Fig. 2.3). All of these miR2111 genes have complementary sequences to *TML* mRNA. Therefore, it is assumed that miR2111 genes that were expressed in leaves have functional redundancies and potentially work in the AON pathway (Fig. 2.2). Indeed, overexpression of *MIR2111-5* and *MIR2111-2*, of which the sequence is 96% identical to that of *MIR2111-7*, significantly increased nodule numbers. In contrast, overexpression of *MIR2111-4* did not affect nodule

numbers; nonetheless, mature miR2111s accumulated at high levels in transformed roots (Fig. 2.4). This may have been due to the atypical secondary structure of miR2111-F derived from *MIR2111-4* (Fig. 2.1b). Unlike the hairpin structures of *MIR2111-2* (Tsikou et al., 2018) and *MIR2111-5*, the mature miR2111 sequence in the predicted miR2111-F secondary structure is located at the 5' end of its stem (Fig. 2.1b). Nucleotide lengths proximal to the miRNA/miRNA* duplex affect the efficiency of correct miRNA processing in *Arabidopsis* (Mateos et al., 2010; Moro et al., 2018; Werner et al., 2010). Although I detected an increase of mature miR2111s in roots overexpressing *MIR2111-4*, miRNA generated from miR2111-F might not have nucleotide sequence patterns that are sufficient to target *TML* mRNA (Fig. 2.4). This notion is supported by the lack of a significant change in *TML* mRNA accumulation in roots overexpressing *MIR2111-4*. Although overexpression of *MIR2111-3* increased nodule numbers in the previous study (Tsikou et al., 2018), expression of *MIR2111-3* was undetectable levels in my RNA-seq of *L. japonicus* leaves (Fig. 2.3). *MIR2111-3* may be expressed under conditions different from those where the other four loci expressed.

It has been proposed that shoot-derived mature miR2111s are translocated to roots via the phloem to enhance nodulation (Tsikou et al., 2018). However, it was unknown whether or not the accumulation of mature miR2111s in shoots leads to an increase in root nodule numbers. I carried out grafting experiments and demonstrated that WT rootstocks grafted with *MIR2111-5* overexpressed scions exhibited increased root nodule numbers and mature miR2111 levels and repressed *TML* mRNA levels (Fig. 2.8a-f). Since the levels of *MIR2111-5* were not increased in WT rootstocks, it is unlikely that the increment in mature miR2111s in rootstocks was due to the movement of *MIR2111-5* from shoots. These results indicated that *MIR2111-5* overexpression in the shoot was sufficient to systemically regulate root nodule numbers and *TML* mRNA levels. Furthermore, results from grafting between *MIR2111-5*ox and AON mutants, *har1-7* and *tml-4*, suggested that *MIR2111-5* functions in the same genetic pathway as these AON factors (Fig. 2.9). In contrast to *MIR2111-5ox*, scions constitutively expressing *proUBQ*:*STTM2111* inhibited the accumulation of mature miR2111s (Fig. 2.10) and decreased nodule numbers in WT rootstocks (Fig. 2.8f). Thus, the shoot-accumulating mature miR2111s influences root nodule numbers in a dose-dependent manner.

Among the seven miR2111 loci, *MIR2111-5* showed the highest level of TPM in *L. japonicus* leaves (Fig. 2.2). When overexpressing in roots, *MIR2111-5* was the most effective at increasing nodule numbers among miR2111 genes I examined (Fig. 2.4). These results

implied that *MIR2111-5* might significantly contribute to the regulation of nodule numbers in *L. japonicus*. Knockout lines of *MIR2111-5* support this notion. Even though there are multiple loci for miR2111 genes in the *L. japonicus* genome (Fig. 2.2; Fig. 2.1a), as for other miRNA gene families in plants (Li and Mao, 2007), a single *mir2111-5* mutation decreased miR2111 levels in leaves and roots to less than half of WT (Fig. 2.11b). In addition, the *MIR2111-5* deletions resulted in the significant inhibition of nodule formation. As for *MIR2111-3* expression patterns (Tsikou et al., 2018), *proMIR2111-5:GUS* expression was observed in the phloem of leaves (Fig. 2.5a, c, d) but not in stems, roots, or nodules (Fig. 2.6). The accumulation of *MIR2111-5* was hardly detected in roots by qRT-PCR (Fig. 2.5h). Considering this expression pattern, it is likely that the decrease in nodule numbers and mature miR2111 levels in roots of *MIR2111-5* knockout lines was caused by the attenuation of mature miR2111 levels in leaves (Fig. 2.11c). The expression in the phloem, which is convenient to explain the shoot-to-root movement of mature miR2111s through the vasculature, was diminished after rhizobial inoculation (Fig. 2.5b). Thus, *MIR2111-5* accumulation in leaves is regulated at the transcriptional level. The decrease in *MIR2111-5* expression in leaves in response to rhizobial inoculation correlated well with the accumulation patterns of mature miR2111s in leaves and roots (Fig. 2.5). The HAR1-dependent transcriptional regulation of miR2111 genes including *MIR2111-5* in leaves would systemically influence nodule numbers in roots. Taken together with the results of grafting experiments, it is likely that mature miR2111s generated in shoots are translocated to roots and post-transcriptionally silence *TML* mRNA.

Phloem sap contains a defined subset of miRNA species and some of these specifically accumulate under various nutrient-limiting conditions (Pant et al., 2008, 2009; Buhtz et al., 2010). In Arabidopsis and tobacco, shoot-to-root mobile miR399s, which accumulate in shoots in response to the deprivation of inorganic phosphate (Pi), post-transcriptionally regulate mRNA for PHO2, which encodes ubiquitin-conjugating E2 enzyme 24 (Lin et al., 2008; Pant et al., 2008). Since PHO2 suppresses Pi uptake in roots, shoot-derived miR399s maintain Pi homeostasis through the regulation of their target mRNA levels. Interestingly, Pi-limitation induces the accumulation of mature miR2111 in rapeseed phloem sap (Buhtz et al., 2010; Pant et al., 2009). Arabidopsis and tobacco miR2111s, which also accumulate in response to Pi-limitation (Huen et al., 2018; Pant et al., 2009), are predicted to target mRNA for *TML* orthologues (Huen et al., 2018). In legumes, the control of miR2111 production depends on nitrate availability (Gautrat et al., 2020; Tsikou et al., 2018). Recently, it has been reported that in *M. truncatula*, nitrogen-deprivation in roots induces the

production of mature miR2111s in shoots through CEP family peptide-mediated long-distance signaling, in order to enhance nodulation (Gautrat et al., 2020). Although the biological functions of *TML* orthologues and roles of miR2111s in Arabidopsis and tobacco have not yet been identified, shoot-derived miRNA accumulation in roots may be a widespread mechanism of adaptation to nutritional changes in plants.

2.4 Methods

Plant materials and bacterial resources

I used *L. japonicus* accession MG-20 (Kawaguchi, 2000) as the WT. *har1-7* (Magori et al., 2009) and *tml-4* (Takahara et al., 2013) mutants were derived from MG-20. *proMIR2111-5*:GUS transgenic lines, *MIR2111-5* overexpression lines, *proUBQ:STTM2111* transgenic lines, and *MIR2111-5* knockout lines were generated in the MG-20 background. *Mesorhizobium loti* MAFF303099 and MAFF303099 constitutively expressing dsRED were used for the *L. japonicus* inoculum.

Plant culture conditions and bacterial inoculation

Sterilized *L. japonicus* seeds were germinated on 0.9% agar medium containing Broughton and Dilworth solution (B&D) (Broughton and Dilworth, 1971) without any nitrogen source for 3 days at 24°C (16 h light, 8 h dark).

For the nodulation and infection phenotyping assay, plants were transplanted on autoclaved vermiculite supplemented with B&D containing 0.5 mM KNO_3 and inoculated with *M. loti* carrying dsRED. Plants were inoculated 3 days after being transplanted and harvested within indicated days after inoculation (dai) to analyze the nodulation and infection phenotypes.

For the RNA-seq, qPCR assay, and promoter GUS assay, plants were transplanted into autoclaved vermiculite containing B&D without a nitrogen source. Plants were inoculated 3 days after being transplanted either with or without *M. loti* carrying dsRED at indicated time points and harvested 14 days after germination.

For the grafting assay, plants were sown on vertical 0.9% agar plates for 2 days in darkness and 2 days under light/dark conditions. The four-day-old seedlings were cut at the basal hypocotyls and shoot scions were grafted on rootstocks as described previously (Magori et al., 2009). Grafted plants were grown horizontally on the sterilized water-absorbed filter paper for 1 week and then transplanted to autoclaved vermiculite containing B&D either with or without 0.5 mM KNO_3 for the nodulation assay and qRT-PCR assay, respectively. Seven

days after being transplanted, grafted plants were inoculated with *M. loti* carrying dsRED and harvested at the indicated time after inoculation.

Plasmid construction

All primers, oligonucleotides, and the synthetic DNA fragment are detailed in Table 2.2.

For the overexpression analyses of *MIR2111-2*, *MIR2111-4*, and *MIR2111-5*, plasmids were constructed as follows. DNA fragments fully covering pri-miR2111 regions, as detected by RNA-seq were amplified from *L. japonicus* ecotype MG-20 genomic DNA by specific primer sets using the PrimeSTAR MAX DNA polymerase (Takara) and cloned into EcoRI-digested pENTR-1A (Invitrogen) using an In-Fusion HD Cloning Kit (Clontech). For hairy root transformation, all inserts were transferred to pUb-GW-GFP (Maekawa et al., 2008) by LR clonase (Invitrogen). The insert of *MIR2111-5* fragment was also transferred to pUb-GW-Hyg (Maekawa et al., 2008) by LR clonase for use in whole plant transformation.

For *proUBQ:STTM2111* construct, the sequence of STTM2111 with attL1 and attL2 was synthesized (attL1:STTM2111:attL2) and cloned into pMA-RQ (GeneArt, Thermo Fisher Scientific). This fragment was cloned into pUb-GW-Hyg by LR clonase.

For the GUS reporter assay of *MIR2111-5*, a 3.0 kb DNA fragment upstream of *MIR2111-5* was amplified from *L. japonicus* ecotype MG-20 genomic DNA using specific primer sets by means of the PrimeSTAR MAX DNA polymerase (Takara) and cloned into EcoRI-digested pENTR-1A (Invitrogen) using an In-Fusion HD Cloning Kit (Clontech). The insert was transferred to pMDC162 (Curtis and Grossniklaus, 2003) by LR clonase.

For CRISPR/Cas9 constructs of *MIR2111-5*, targeting sites were designed using the CRISPR-P 2.0 program (Liu et al., 2017). Two gRNAs were used for each construct to delete a nearby miR2111a sequence in *MIR2111-5* on the *L. japonicus* genome. In order to create CRISPR/Cas9 constructs containing dual gRNA, I first modified the gRNA cloning vector pMR203 (provided by Dr. Mily Ron and Dr. Masaki Endo) as follows. DNA fragments of U6-26 promoter/BbsI/Chimera RNA (sgRNA) were amplified by two types of specific primers with multiple cloning sites (MCS) using the PrimeSTAR GXL DNA polymerase (Takara) from pMR203. Each DNA fragment was inserted between the ApaI and PstI sites of pMR203 to create new cloning vectors with different MCS, designated as pMR203_AB and pMR203_BC, which enable a removal of a gRNA expression cassette after cloning of gRNA using standard restriction enzymes. The binary vector pMR285 (derived from pDe-Cas9) (Ritter et al., 2017) was also modified as follows. Two oligo DNAs, forward and reverse of pMR285_oligo (Table 2.2), were annealed and inserted into the BbsI site of pMR203 to

create MCS. The DNA fragment of this MCS was removed by PstI and inserted into the PstI site of pMR285 to create new binary vectors with MCS, designated as pMR285_AD. Then, oligonucleotide pairs for gRNA were annealed at 95 °C for 5 min and inserted into the BbsI site of pMR203_AB and pMR203_BC. The gRNA expression cassettes in pMR203_AB and pMR203_BC were removed using BamHI/SalI and SalI/XbaI, respectively. These fragments were inserted simultaneously between the BamHI and XbaI sites of pMR285_AD.

Plant transformation

Whole-plant transformation of *L. japonicus* was performed using *Agrobacterium tumefaciens*-mediated method as described previously (Nishida et al., 2018). *A. tumefaciens* AGL1 strains carrying the plasmid of interest were cultured in LB liquid medium supplemented with appropriate antibiotics at 28°C for 2 days. The seedlings of *L. japonicus* grown on the 0.9% agar medium containing B&D (24°C dark for 3 days) were placed on sterilized filter papers (6 x 6 cm) impregnated with the prepared *A. tumefaciens* suspension and their hypocotyl were cut to approximately 3 mm segments. The hypocotyl segments were transferred onto 5 mm piles of sterilized filter papers (6 x 6 cm) supplemented with co-cultivation medium (1/10 Gamborg's B5 salt mixture, 1/10 Gamborg's vitamin solution, 0.5 μg mL^{-1} BAP, 0.05 μg mL^{-1} NAA, 5 mM MES (pH 5.2), 20 μg ml^{-1} acetosyringone, pH 5.5) and cultured for 3 days at 24°C dark to facilitate the infection of *A. tumefaciens* to the hypocotyl segments. Then, the hypocotyl segments were transferred onto a callus induction medium (Gamborg's B5 salt mixture, Gamborg's vitamin solution, 2% sucrose, 0.2 μg mL^{-1} BAP, 0.05 μg mL^{-1} NAA, 10 mM $(NH_4)_2SO_4$, 12.5 μg mL^{-1} meropenem, 20 μg mL^{-1} Hygromycin B, 0.6% agar, pH 5.5) and cultured for 2-5 weeks at 24°C (16 h light, 8 h dark). The hypocotyl segments were transferred onto a new callus induction medium every 5 days. The developed-calli were placed on the callus induction medium without Hygromycin B to induce primordia of adventitious shoot for 3–7 weeks at 24°C (16 h light, 8 h dark). The calli were transferred onto a new medium every 5 days. When primordia of adventitious shoot became visible in calli, the calli were transferred onto a shoot elongation medium (Gamborg's B5 salt mixture, Gamborg's vitamin solution, 2% sucrose, 0.2 μg ml^{-1} BAP, 12.5 μg mL^{-1} meropenem, 0.6% agar, pH 5.5) and grown for 3–6 weeks at 24°C (16 h light, 8 h dark) to elongate shoot from leaf primordia. The calli were transferred onto a new callus induction medium every 7 days. The individual shoots from calli were detached and inserted into a root induction medium (1/2 Gamborg's B5 salt mixture, 1/2 Gamborg's vitamin solution, 1% sucrose, 0.5 μg ml^{-1} NAA, 0.9% agar, pH 5.5) and cultivated for 10 days at 24°C (16 h light,

8 h dark). Then, they were inserted into root elongation medium (1/2 Gamborg's B5 salt mixture, 1/2 Gamborg's vitamin solution, 1% sucrose, 0.9% agar, pH 5.5) and grown until their root length became more than 3 cm. The generated transgenic plants were transplanted into vermiculite to obtain their seeds.

Hairy root transformation of *L. japonicus* roots was performed using *Agrobacterium rhizogenes*-mediated transformation as described previously (Nishida et al., 2018). *A. rhizogenes* AR1193 strains carrying the plasmid of interest were grown on YEB medium containing 1.5% agar supplemented with appropriate antibiotics at 28°C for 2 days. *A. rhizogenes* AR1193 strains were collected and suspended in 6 mL sterilized water. The seedlings of *L. japonicus* were grown on a 0.9% agar medium containing B&D for a total of 3 days (darkness for 2 days and 16 h light, 8 h dark for 1 days). The seedlings were placed in the *A. rhizogenes* suspension and cut in the middle of their hypocotyls. The seedlings without roots were placed on a co-cultivation medium for hairy root transformation (1/2 Gamborg's B5 salt mixture, 0.01% sucrose, 0.9% agar, pH 5.5) for 3 days (24°C darkness). Then, they were transferred onto vertical hairy root induction medium (Gamborg's B5 salt mixture, Gamborg's vitamin solution, 1% sucrose, 12.5 μg mL^{-1} meropenem, 0.9% agar, pH 5.5) and grown for 10 days at 24°C (16 h light, 8 h dark). The plants with transformed roots displaying fluorescence of a GFP transformation marker were selected and used for further analyses.

GUS staining

Two-week-old *proMIR2111-5:GUS* introduced transgenic plants were incubated with ice-cold 90% acetone on ice for 10 minutes and then stained with GUS staining buffer (0.4 mg mL^{-1} X-Gluc, 50 mM phosphate buffer pH7.0, 1 mM $K_4[Fe(CN)_6]$, 1 mM $K_3[Fe(CN)_6]$, and 0.1% Triton X-100) at 37°C for 3 h. Stained plants were incubated at 37°C for 1 h with acetic acid and ethanol (ratio 6:1) buffer to remove the chlorophyll background.

Microscopic observation

An SZX16 stereomicroscope or a BX50 microscope (Olympus) was used to observe roots, nodules, and GUS-stained whole plants. Nodules with the neck at the basal region were counted in nodulation phenotype assays. For plastic sections, GUS-stained leaves, stems, or nodules were fixed with Formalin-Acetic-Alcohol buffer for 12 h at 4°C and embedded in Technovit 7100 resin (Haraeus Kulzer). Sections were cut with a microtome RM2255 (Leica) at a thickness of 5 μm and counterstained with 0.1% safranin for 10 minutes at 55°C.

Library preparation and sequencing

Total RNA was extracted from true leaves of *L. japonicus* grown under the conditions described using PureLink Plant RNA Reagent (Thermo Fisher Scientific) and purified using RNeasy Plant Mini Kit (Qiagen). The quality of RNA was evaluated using an Agilent 2100 Bioanalyzer with Agilent RNA 6000 Nano kit. RNA-seq libraries were prepared using NEBNext Ultra II RNA Library Prep Kit for Illumina (New England Biolabs) according to the manufacturer's protocol. The prepared RNA-seq libraries were qualified by the Agilent 2100 Bioanalyzer using Agilent High Sensitivity DNA kit and quantified using a KAPA Library Quant Kit (Kapa Biosystems). Each library was diluted to 2 nM. Libraries were sequenced using NextSeq 550 (Illumina) and generated 81 bp single-end reads.

Bioinformatic analysis

All acquired RNA-seq reads were qualified by FastQC (ver. 0.11.7) and adapter trimmed by Trimomatic (Bolger et al., 2014) (ver. 0.36, options: CROP:80 LEADING:30 TRAILING:30 SLIDINGWINDOW:4:15 HEADCROP:6 MINLEN:36). Trimmed reads were mapped to the *L. japonicus* genome (Gifu v1.2) using Hisat2 (ver. 2.1.0) (Kim et al., 2019). The mapped reads with a MAPQ score of less than 30 were filtered out using SAMtools (v1.9, options: view -bq 30) (Li et al., 2009) to handle only high mapping quality scored reads for downstream analysis. The number of raw reads, trimmed reads, and mapped reads are shown in Table 2.3. Filtered mapped reads were assembled and calculated TPM values using Stringtie (ver. 1.3.4d) (Pertea et al., 2015) with the default setting. To visualize read coverage in the Integrative Genomics Viewer (ver. 2.4.10) (Robinson et al., 2011), filtered mapped reads were normalized by bins per million mapped reads (BPM) using bamCoverage (ver. 3.3.1, options: --binSize=10 --normalizeUsing BPM --smoothLength 30) (Ramírez et al., 2016).

In order to predict new miR2111 loci, I searched miR2111a, b, and c sequence from new *L. japonicus* genome assembly (Gifu v1.2) by BLASTn (Camacho et al., 2009). I identified a total of 10 positions for miR2111a, miR2111b, or miR2111c from the *L. japonicus* genome. 100 bp-upstream and -downstream sequences from the identified 21 bp miR2111 regions were extracted and the secondary structure was predicted using minimum free energy (MFE) algorithm of RNAstructure program (ver. 6.1) (Reuter and Mathews, 2010). Next, I searched for pri-miR2111s expressing in *L. japonicus* using mapped my RNA-seq data. In order to detect pri-miR2111 expression from my RNA-seq data, RNA-Seq-based

gene predictions were performed using Stringtie (ver. 1.3.4d) with the default setting. I then searched for pri-miR2111s from predicted potential *L. japonicus* genes based on my RNA-seq data by referring to the position of the miR2111 hairpin sequences including those I predicted. Furthermore, I searched new potential miR2111 genes that were not detected in my RNA-seq data using BLASTn search of sequences for all miR2111 genes against the *L. japonicus* genome and identified one new potential miR2111 gene. Secondary structures of all new miR2111s were re-estimated using the full-length sequence of the predicted miR2111 genes using the MFE algorithm of RNAstructure (ver. 6.1). The genomic positions of miR2111s were visualized by R software (ver. 3.6.2) with chromoMap package (ver. 0.2) (Anand and Lopez, 2020).

Phylogenetic analysis of miR2111 genes

Putative miR2111 genes were aligned with MAFFT (ver. 7.313) (Katoh et al., 2002) with default parameters. Aligned sequences were trimmed using trimAL (ver. 1.4.rev22, option: -automated1) (Capella-Gutiérrez et al., 2009). Phylogenetic trees were constructed by maximum likelihood (ML) analysis with IQ-TREE (ver. 1.6.9) (Nguyen et al., 2015). ML tree was visualized using R software (ver. 3.6.2) with ggtree package (ver. 1.14.6) (Yu et al., 2017).

qRT-PCR analysis

Total RNA including miRNA was extracted from either roots or true leaves of plants grown under the conditions described using NucleoSpin miRNA (MACHEREY-NAGEL Inc). For qRT-PCR of mRNA and miR2111 precursors, extracted RNA was reverse-transcribed using PrimeScript RT reagent Kit (Perfect Real Time) (Takara). Mature miR2111s were reverse-transcribed and adapter-ligated using the Mir-X miRNA First-Strand Synthesis Kit (Takara). Mature miR2111-specific primer and adapter-specific primer contained in Mir-X miRNA First-Strand Synthesis Kit were used for the amplification of mature miR2111s. qRT-PCR was carried out by LightCycler 96 (Roche Applied Science) using TB Green Advantage qPCR Premix (Takara). *Ubiquitin* and *ATP synthase* were used for normalization of expression levels. Primers of *Ubiquitin* (Nagae et al., 2016) and *ATP synthase* (Tsikou et al., 2018) were synthesized as described previously. All primers are listed in Table 2.2.

Statistical analysis

Tukey's honestly significant difference test (Tukey-HSD) was performed with R software (ver. 3.6.2). Two-sided Student's *t*-test was performed by Python (ver. 3.6.7) with SciPy library (ver. 1.1.0).

Data availability

The raw RNA-seq reads have been deposited in the DDBJ Sequence Read Archive (DRA) under accession number DRA009878.

Chapter 3

"Transcriptomic and phenotypic characterization of the shoot during systemic control of nodulation"

3.1 Introduction

As described in Chapter 1, root-shoot-root signaling-mediated adaptation to fluctuating soil nutrients is an important mechanism for land plants. In Arabidopsis, miR399s accumulate in the shoot in response to inorganic phosphate deficiency in roots. These miR399s are translocated from the shoot to the roots to increase inorganic phosphate uptake (Lin et al., 2008; Pant et al., 2008). Under heterogeneous soil nitrate availability, root-to-shoot mobile CEP peptides are synthesized in roots in response to local nitrate deprivation. The root-derived CEP peptides are recognized by the shoot-acting receptors CEPR1 and CEPR2, and then enhance nitrate uptake in roots in nitrate-rich soil through root-to-shoot mobile signals, CEPD1 and CEPD2 (Ohkubo et al., 2017; Tabata et al., 2014). Although the physiological functions of these signaling in the roots, namely the sensing of nutrient deficiencies and the promotion of nutrient absorption, have been elucidated, it is unclear why these signaling need to be transmitted via the shoot.

As described above, legumes also adopt the mechanism of root-shoot-root signaling transduction, known as AON, to restrict root nodule numbers (Caetano-Anollés and Gresshoff, 1991; Suzaki et al., 2015). In the current model of AON in *L. japonicus*, root-derived mobile signals, CLE-RS1, RS2, and RS3 peptides, are induced in roots by either inoculation of rhizobia or treatment with nitrate (Nishida et al., 2016; Okamoto et al., 2013b, 2009). These CLE peptides are transported to the shoot via the xylem vessel and are perceived by a shoot-acting HAR1 receptor-like kinase (Okamoto et al., 2013b). Then, the root-acting factor, *TML* encoding F-box protein inhibits nodulation (Magori et al., 2009; Takahara et al., 2013). It has been reported that HAR1 induces the synthesis of cytokinin in the shoot through the expression of *IPT3* (Sasaki et al., 2014). This shoot-derived cytokinin inhibits nodulation via *TML*. In addition to cytokinin, miR2111, which targets *TML* mRNA, has been identified as another shoot-derived downstream factor in HAR1 controlling nodulation (Gautrat et al., 2020; Okuma et al., 2020; Tsikou et al., 2018). The precursors of miR2111 expressed along the phloem of leaves and the shoot-derived miR2111 systemically increase root nodule numbers through a decrease in *TML* mRNA abundance in roots.

As in other root-shoot-root signaling cases, the physiological functions of AON in roots are well known, but it is unclear why AON acts through shoot-mediated signaling. In a previous study, it was reported that soybean mutants of NARK, an orthologue of HAR1, have smaller leaf size and leaf cell numbers than the WT (Ito et al., 2008), indicating that AON may have functions other than the regulation of nodulation, such as the promotion of shoot growth. To fully understand how legumes adapt to rhizobial infection and changes of nitrate availability at the whole plant level using AON, it is necessary to elucidate the role of AON in the shoot, other than to produce shoot-derived factors controlling nodulation. In this study, I focused on the genes regulated by HAR1 in the leaves on the AON pathway to gain new insights that will contribute to the elucidation of this unanswered question.

3.2 Results

IPT3 is mainly expressed in the vascular bundle of mature leaves in a HAR1-dependent manner

Although reciprocally grafted *har1* mutants showed that HAR1 acts in the shoot with respect to the control of nodule numbers, the expression of *HAR1* is detectable in both the roots and the shoot vascular bundle and its expression is stable whether inoculated with rhizobia or not (Nontachaiyapoom et al., 2007). To characterize responsive genes downstream of *HAR1*, it is necessary to determine the precise functional site of HAR1 in the shoot. Since HAR1 induces *IPT3* expression in leaves in response to rhizobial infection and nitrate treatment (Sasaki et al., 2014), I used *IPT3* expression pattern as a reference for the putative functional site of HAR1 in the shoot.

To evaluate the spatial expression patterns of *IPT3*, I used *IPT3* promoter GUS transgenic lines (*proIPT3:GUS*) (Sasaki et al., 2014) in the WT background. I also generated *proIPT3:GUS* transgenic lines in the *har1-7* background (*har1-7 proIPT3:GUS*) to evaluate the dependency of the spatial expression of *IPT3* on HAR1. Histochemical GUS staining analyses using *proIPT3:GUS* transgenic lines showed that *IPT3:GUS* expression was induced in the vascular bundle of true leaves in response to either rhizobial inoculation or 5 mM KNO_3 treatments in the WT background (Fig. 3.1a-c). In addition, stronger GUS signals were detected in older leaves compared with younger leaves (Fig. 3.1a-c). Since the GUS signal was almost undetectable in leaves of *har1-7 proIPT3:GUS* plants, rhizobial infection- or nitrate-responsive *IPT3* expression along the leaf vascular bundle depended on HAR1. Next, I evaluated the induction timing of *IPT3* in older true leaves by qRT-PCR analysis. The results showed that *IPT3* was induced in 1 day after either rhizobial inoculation or 5 mM

KNO_3 treatments depending on HAR1 (Fig. 3.1d). These spatial and temporal expression patterns of *IPT3* were very similar to those of miR2111 precursor genes, which are regulated by HAR1 (Okuma et al., 2020; Tsikou et al., 2018), suggesting that the functional site and timing of HAR1 in shoots is likely to be the vascular bundles of older true leaves within 1 day after rhizobial inoculation or nitrate treatment.

HAR1 and *CLE-RS1/2* may induce photosynthesis-related gene expression

Next, I carried out RNA-seq analyses of *L. japonicus* leaves to characterize the downstream genes of HAR1. Two-week-old seedlings of WT, *har1-7*, *CLE-RS1*ox, and *CLE-RS2*ox were prepared for RNA-seq analyses. WT and *har1-7* were treated with either mock, rhizobial inoculation, or 5mM KNO_3. *CLE-RS1*ox and *CLE-RS2*ox were only treated with mock. Total RNA was sampled from the true leaves of these plants, where the stronger GUS signal of *IPT3* was detected (Fig. 3.1a-c), for RNA-seq.

I searched for genes whose expression was induced compared to the mock treatments. Overall, a total of about 10,000 upregulated genes were detected. 261 genes were found to be commonly upregulated due to *CLE-RS1*/*2* overexpression as well as either rhizobial inoculation or nitrate treatment in a HAR1-dependent manner (Fig. 3.2a; Table 3.1). To investigate the functional relevance of these genes, gene ontology (GO)-enrichment analysis was carried out. I found that most enriched GO terms were involved in the electron transport of respiration and photosynthesis (Fig. 3.2b). These genes with enriched GO terms were encoded PSII proteins (*psbB* and *psbH*) and cytochrome *b6f* subunits (*petB*, *petD*), implying that HAR1 somehow influenced the mRNA levels of genes encoding proteins involved in electron transport during photosynthesis (Table 3.1). In addition, *stomagen*, which positively regulates the differentiation of stomatal lineage cells into stomata, was upregulated in a HAR1-dependent manner (Table 3.1). The upregulation of these genes with enriched GO terms was observed in the leaves of WT plants treated with 5 mM KNO_3 and in *CLE-RS1* or *RS2* overexpressing plants, but not in leaves of WT treated with rhizobial inoculation. Based on these results, I hypothesized that HAR1 somehow influences photosynthetic activity in leaves in response to high concentrations of nitrate and either *CLE-RS1* or *RS2* overexpression.

***har1-7* mutant has a lower *Fv/Fm* value and starch accumulation in leaves compared with WT.**

To evaluate the effects of *har1-7* mutation on photosynthesis, chlorophyll fluorescence was analyzed using pulse-amplitude-modulation (PAM) chlorophyll fluorometer. WT, *har1-7*, and *CLE-RS1*ox were cultivated for about a month, supplemented with 10 mM KNO_3 containing B&D medium for this analysis. *har1-7* mutant showed a significantly lower *Fv/Fm* ratio, which can be approximated to the maximum quantum yield of PSII, implying that *har1-7* possibly defect normal regulation of photosynthetic activity (Fig. 3.3a). I further evaluated the photosynthesis-related phenotypes of *har1-7* by analyzing starch accumulation in the shoots. For starch staining, WT and *har1-7* were cultivated for two weeks with 1 mM KNO_3 containing B&D. I found that the accumulation of stained starch in *har1-7* was seemingly lower than that in WT (Fig. 3.3b).

3.3 Discussion

To maintain root nodule symbiosis, it is necessary to balance between the production of photosynthate in leaves and the fixation of nitrogen in roots. In this study, I characterized the downstream factors of HAR1 by transcriptome analyses in the leaves to elucidate the adaptive implication of shoot-mediated regulation. I found that HAR1 influenced transcript abundance of photosynthesis-related genes, *Fv/Fm*, and starch accumulation patterns in leaves. Therefore, in addition to controlling the number of nodules, HAR1 may promote the supply of carbon required for symbiosis with rhizobia or nitrogen assimilation by enhancing photosynthetic activity in the shoot. Since few reports have described the function of AON in the shoot other than the control of nodule numbers, this study may provide a clue to answer the question of why root nodule symbiosis is controlled by the shoot.

To date, only two genes whose expression in leaves is controlled by HAR1 (*IPT3* and miR2111) have been reported. From the RNA-seq analyses, I found more than 200 genes that were commonly upregulated in leaves by nitrate treatment and *CLE-RS1* or *RS2* overexpression in a HAR1-dependent manner (Fig. 3.2a). On the other hand, there were very few genes that are commonly induced by rhizobial inoculation and *CLE-RS1* or *RS2* overexpression (Fig. 3.2a), indicating that the treatment with 5 mM KNO_3 can more strongly regulate the induction of HAR1 downstream genes through activation of *CLE-RS1*/*2* expression than that of rhizobial inoculation. The results of GO-enrichment analysis on upregulated genes depending on HAR1 showed significant enrichment of photosynthesis-related GO terms (Fig. 3.2b; Table 3.1). All differentially expressed genes with photosynthesis-related GO terms were encoded by the chloroplast genome. Chloroplastic gene mRNA levels generally do not rely on transcription rate. Post-transcriptional RNA

processing and stabilization have an important role in the accumulation of chloroplastic gene mRNA (del Campo, 2009). HAR1 possibly regulates steps of post-transcriptional RNA processing. Since these upregulated chloroplastic genes contained only part of components of PSII complex and cytochrome *b6f* complex, it is difficult to discuss the implications of differences in expression patterns for photosynthetic complexes within the thylakoid membrane. Further analyses of the protein levels and translation activity of photosynthetic electron transport system components, as well as the effects on actual photosynthetic electron transfer reactions, are needed for understanding these results.

Mutation of *har1-7* seemed to negatively influence photosynthetic activity. *har1-7* showed a lower maximum quantum yield of primary PSII photochemistry, as determined by *Fv/Fm* testing, compared with WT. The optimal value of *Fv/Fm* is approximately in the range of 0.78–0.84 in various plant species, while light irradiation or abiotic stress, such as salinity, decreases *Fv/Fm* (Tsai et al., 2019). Since there was no great difference between *Fv/Fm* in WT (0.76 on average) and the optimal value, the lower *Fv/Fm* ratio of *har1-7* (0.53 on average) may not be due to the stress caused by growth conditions. Thus, *har1-7* may have some defects in the normal control of photosynthesis. In addition to the significantly lower *Fv/Fm* of *har1-7*, *har1-7* accumulated seemingly less starch in their shoots than those of WT. These results support my hypothesis that HAR1 influences photosynthetic activity. In the future studies, It needs to be examined whether HAR1 does in fact affect photosynthetic activity. Also, it will be necessary to determine what downstream factors of HAR1 are involved in differences in photosynthesis-related phenotypes observed in *har1-7*.

3.4 Methods

Plant materials and bacterial resources.

Lotus japonicus accession MG-20 (Kawaguchi, 2000) was used as the WT. *har1-7* (Magori et al., 2009) was derived from MG-20. *Mesorhizobium loti* MAFF303099 constitutively expressing dsRED was used as the *L. japonicus* inoculum. *proIPT3*:GUS transgenic lines, *CLE-RS1*, and *RS2* overexpression lines in WT background were generated in a previous study (Sasaki et al., 2014). *har1-7 proIPT3*:GUS transgenic lines were generated by stable transformation with the *proIPT3*:GUS reporter construct.

GUS staining

Two-week-old *proIPT3*:*GUS* transgenic plants were sampled and stained as described in Chapter 2.4.

Plant culture conditions and bacterial inoculation

Sterilized *L. japonicus* seeds were germinated on 0.9% agar medium containing Broughton and Dilworth solution (B&D) (Broughton and Dilworth, 1971) without any nitrogen source for 3 days at 24°C (16 h light, 8 h dark).

For the RNA-seq and promoter GUS assays, plants were transplanted into autoclaved vermiculite containing B&D without nitrogen sources. Plants were inoculated at indicated time points either with or without *M. loti* carrying dsRED and harvested 14 days after germination.

Library preparation and sequencing

Total RNA was extracted from true leaves of WT, *har1-7*, *CLE-RS1*ox, and *CLE-RS2*ox plants grown under the conditions described, using PureLink Plant RNA Reagent (Thermo Fisher Scientific) and purified using the RNeasy Plant Mini Kit (Qiagen). Library preparation and sequencing were performed as described in Chapter 2.4.

***Fv/Fm* measurements using pulse-amplitude-modulation (PAM) chlorophyll fluorometer**

Leaves of WT, *har1-7*, and *CLE-RS1*ox that were cultivated after a month of being supplied with 10 mM KNO_3 containing B&D medium were sampled for this analysis. As one replicate, three fully expanded leaves were sampled from an individual plant. *Fv/Fm* ratio was measured using the Walz PAM-2100.

Starch staining

Shoots of WT and *har1-7* that were cultivated for two weeks supplied with 5 mM KNO_3 containing B&D medium were sampled for this analysis. Shoots were incubated at 37°C for 1 h with acetic acid and ethanol (ratio 6:1) buffer to remove the chlorophyll background. Starch was stained with 0.03% potassium iodide for 1 min.

Chapter 4

“General discussion”

Functions of plant shoot-to-root mobile microRNA in the adaptation to fluctuating soil nutrient availability

Phloem sap contains various miRNAs, the accumulation levels of which are regulated by the limitation of nutrients available for plants, implying that shoot-to-root mobile miRNAs may play a crucial role in adaptation to nutritional fluctuations (Buhtz et al., 2010; Pant et al., 2009, 2008). Indeed, inorganic phosphate (Pi)-limitation-responsive miRNA, miR399, moves from the shoot to the roots and increases Pi uptake through the target mRNA degradation in roots (Pant et al., 2008). Although many studies have shown shoot-to-root translocation of miRNA species, there are only a few examples of mobile miRNAs, such as miR399, whose detailed molecular functions have been revealed (Pagliarani and Gambino, 2019). As described in Chapter 2, I clearly showed that miR2111 is produced in leaves and is a graft-transmissible signal that enhances nodulation in the roots. *MIR2111-5* locus plays an important role in the production of miR2111 in leaves and the enhancement of nodulation since *mir2111-5* mutants decrease miR2111 levels and the number of nodules. The further functional characterization of shoot-derived miR2111 in Chapter 2 may contribute to further understanding of the environmental adaptation strategy of plants, especially to nutrient deficiency, through shoot-root transfer of miRNA species.

The role of miR2111 in symbiotic interactions and inorganic phosphate (Pi) responses

In Arabidopsis, tobacco, and rapeseed, it has been reported that miR2111s accumulates in response to Pi-deficiency. In addition, the results of grafting experiments of Arabidopsis and deep sequencing of rapeseed phloem sap have demonstrated that miR2111s have shoot-to-root mobility (Buhtz et al., 2010; Pant et al., 2009). Since miR2111 targets mRNA of the *TML* orthologous gene in Arabidopsis and tobacco, the miR2111-*TML* relationship is likely conserved in non-legumes (Huen et al., 2018). Although the functions of the miR2111-*TML* module in non-legumes remain unclear, it may have a function related to the responsiveness of miR2111s to Pi. One possibility is that miR2111 may be involved in symbiosis with arbuscular mycorrhizal fungi (AMF) (Oldroyd and Leyser, 2020). Approximately 80% of land plants establish symbiotic relationships with AMF and take advantage of nutrient acquisition, especially Pi, through AMF. AM symbiosis is evolutionarily older than legume-

Rhizobium symbiosis and many of the regulatory mechanisms of AM symbiosis are diverted to regulate legume-*Rhizobium* symbiosis (Markmann and Parniske, 2009). In *M. truncatula*, specific CLE peptides are induced in roots in response to high Pi and inhibit colonization of AMF through shoot-acting SUNN receptor-like kinase, an orthologue of *L. japonicus* HAR1 (Karlo et al., 2020; Müller et al., 2019). Considering that SUNN regulates miR2111 accumulation in the AON pathway (Gautrat et al., 2020), the AMF colonization rate may also be regulated via miR2111 downstream of the *CLE-SUNN* interaction.

The responsiveness of miR2111 to nitrate is different between legumes and Arabidopsis (Gautrat et al., 2020; Liang et al., 2015; Tsikou et al., 2018). The accumulation of miR2111 is increased by nitrate deficiency in legumes, whereas it is decreased in Arabidopsis. A possible explanation for this discrepancy may lie in the distinctions in the shoot-derived factors of the CEP-CEPR module downstream, the long-distance signaling components that inform nitrate starvation (Gautrat et al., 2020; Ohkubo et al., 2017). In Arabidopsis, after CEP is perceived by the CEPR1 and CEPR2 in the shoot, CEPD1 and CEPD2 are induced and systemically promote root nitrate uptake (Ohkubo et al., 2017; Tabata et al., 2014). On the other hand, in *M. truncatula*, Compact Root Architecture 2, an orthologue of Arabidopsis CEPR1, induces miR2111 accumulation in the shoot and systemically promotes nodulation under nitrate starvation (Gautrat et al., 2020). The recruitment of miR2111 in the nitrate starvation response through the CEP-CEPR module might have contributed to the gain of root nodule symbiosis in legumes.

miR2111 is hypothesized to be involved in the control of both root nodule and AM symbiosis (Oldroyd and Leyser, 2020). However, miR2111 is conserved in Brassicaceae such as Arabidopsis and rapeseed (Pant et al., 2009), even though they lack the ability of both root nodule symbiosis and AM symbiosis. Thus, there may be more general functions in miR2111, perhaps related to the Pi responses, which are different from the control of symbiosis. In other words, miR2111 in Brassicaceae may have a narrower function than that in legumes. Indeed, Arabidopsis and rapeseed only have two copies of miR2111, although *L. japonicus*, *M. truncatula*, and soybean have seven, 15, and six copies of miR2111, respectively (Gautrat et al., 2020; Okuma et al., 2020; Zhang et al., 2021). These differences in the degree of duplication in miR2111 may be correlated to the diversity of miR2111 functions. Given that many nutrient-responsive genes have been evolutionarily diverted to the regulation of root nodule and AM symbiosis (Kim et al., 2020; Roy et al., 2020), elucidation of the function of miR2111 and *TML* in Brassicaceae may provide novel insights into how

regulatory mechanisms of root nodule and AM symbiosis were acquired from pre-existing nutrient response mechanisms.

In Chapter 2, I identified all *L. japonicus* miR2111 loci in the latest version of genome assembly (Gifu v1.2) and showed four loci were expressed in the leaves at different levels. The miR2111 loci, the expression of which was not observed in the leaves, could have functions that are distinct from nodulation control. This notion is supported by a study of soybean miR2111. The expression of some miR2111 loci in soybean did not depend on rhizobial infection (Zhang et al., 2021). Functional characterization of the rhizobial infection-independent miR2111 loci might be a clue to resolving the unknown roles of miR2111 in non-legume plants.

The role of root-shoot-root signaling in the shoot: in the case of AON

As mentioned above, plants adapt to nutrient deficiencies in the root via the root-shoot-root long-distance signaling mechanisms. Although the physiological functions and the molecular mechanism of these signalings in the roots have been identified, how these signal transduction pathways to shoot directly influence the shoot growth and metabolism remain unclear. AON is also achieved through root-shoot-root long-distance signaling transduction. In AON-defective mutants such as *har1*, symbiotic interactions with rhizobia severely inhibit shoot growth, which has been explained mainly by excessive nodule formation in the roots. On the other hand, since AON is a signal transduction through the shoot, some functional defects in mutants such as the regulation of shoot growth and metabolism may also be the cause of growth inhibition. As shown in Chapter 3, I found that HAR1 induced the genes involved in photosynthesis in response to nitrate treatment and *CLE-RS1*/*2* overexpression. Furthermore, I found that *har1-7* exhibited a significantly lower *Fv/Fm* ratio and tended to accumulate less starch in their leaves compared to WT. Therefore, in addition to its function in controlling the number of nodules, I hypothesize that HAR1 regulates photosynthetic activity in the leaves. Legumes may regulate root nodule symbiosis at the whole plant level via AON by regulating the synthesis of photosynthate, which is essential for the maintenance of nodules. This study could contribute not only to the understanding of the mechanism of AON in legumes, but also provide new insight into the understanding of environmental adaptation strategies via root-shoot-root long-distance signaling in land plants.

Systemic coordination of carbon and nitrogen assimilation: Evolutionary origin of AON?

Photosynthesis requires large amounts of nitrogen metabolites to maintain photosynthetic machinery proteins. In contrast, assimilation of nitrogen, which is acquired from the soil, depends greatly on photosynthesis because it requires the supply of carbon skeletons as acceptors of inorganic nitrogen to synthesize amino acids, and ATP and NAD(P)H as energy. Therefore, plants tightly coordinate the rate of carbon and nitrogen metabolic assimilation (Nunes-Nesi et al., 2010). For instance, light irradiation promotes nitrate uptake and nitrogen assimilation (Masclaux-Daubresse et al., 2010). It has been reported that HY5, a shoot-to-root mobile transcription factor, is involved in the systemic regulation of nitrogen acquisition (Chen et al., 2016; Masclaux-Daubresse et al., 2010). Conversely, photosynthetic activity is regulated by the nitrogen nutrient status of the roots (Horchani et al., 2010; Shao et al., 2020). However, the molecular mechanisms underlying this root-to-shoot systemic regulation of photosynthetic activity remain unclear. As from results in Chapter 3, I proposed a hypothesis that HAR1 in the shoot may influence photosynthesis in response to nitrate nutrition. If this hypothesis is proven in the future, the results in Chapter 3 could be the first clue to reveal the molecular mechanism in land plants for the root-to-shoot systemic regulation of photosynthetic activity in response to nitrogen availability. Further understanding of AON may provide new insight into the molecular basis of the regulatory mechanisms of carbon fixation in response to external nitrogen availability.

In terms of the regulation of legume-*Rhizobium* symbiosis, AON is believed to play a crucial role in maintaining carbon and nitrogen metabolites balance by restricting nodule numbers. The possible function of HAR1 regulating photosynthetic activity in response to nitrate states, implies that AON may maintain the balance of carbon and nitrogen metabolites, regardless of the symbiotic/non-symbiotic state. Considering that the genes involved in AON (such as *HAR1*, *TML*, *CLE*, and *PLENTY*) are widely conserved in land plants, AON may have been acquired from an unknown pre-existing system controlling carbon and nitrogen balance that is extensively adopted in land plants. Interestingly, a CLE peptide in Arabidopsis, CLE2, may play a role in the systemic regulation of the balance of carbon and nitrogen metabolites like the *HAR1–CLE-RS1/2* module (Ma et al., 2020). RNA-seq analysis revealed that induction of *CLE2* expression in roots systemically induced the expression of several genes involved in light-dependent carbohydrate metabolism in the shoot. Note that of all Arabidopsis *CLE* genes, the CLE domain sequence of *CLE2* shows the highest level of identity with those of *CLE-RS1* and *RS2* (only one difference in amino acid sequence)

(Okamoto et al., 2009). Since *CLE2* expression in roots is induced by nitrate treatment (Ma et al., 2020; Scheible et al., 2004), there could be an evolutionary link to the function of *HAR1–CLE-RS1/2* module. Investigation of the detailed molecular mechanisms underlying *HAR1–CLE-RS1/2* or *CLE2* function involved in carbon metabolism could provide new insight into how land plants maintain homeostasis of carbon and nitrogen metabolism under fluctuating nitrogen availability at the whole plant level. In addition, this knowledge will contribute to unravelling the evolutionary history of the acquisition of regulatory mechanisms of legume-*Rhizobium* symbiosis.

The potential role of AON study in sustainable agriculture

As mentioned in Chapter 1, the production of chemical nitrogen fertilizer, namely industrial nitrogen fixation, consumes fossil fuels, and thus generates a huge amount of carbon dioxide. In contrast, legumes fix atmospheric nitrogen using carbon dioxide via photosynthesis. Therefore, the effective use of legume-*Rhizobium* symbiosis is a suitable strategy to accomplish sustainable agriculture, not only in terms of reducing nitrogen fertilizer usage but also for carbon sequestration. AON has been widely studied as an agronomically important mechanism because it is considered to play a crucial role in optimizing root nodule numbers. As seen in the severe growth inhibition of the nodulated *har1* mutant, AON may be a necessary mechanism for adequate growth of legumes in the presence of rhizobia. I showed that HAR1 may also have a function in regulating photosynthetic activity. This means that AON may contribute to carbon sequestration in two ways: by regulating legume-*Rhizobium* symbiosis and by promoting photosynthesis. Therefore, elucidating the detailed molecular mechanisms of how AON is involved in the regulation of photosynthetic activity may help to develop superior legume varieties that will contribute to the achievement of sustainable agriculture for atmospheric carbon dioxide reduction in the future.

References

Anand, L., Lopez, C.M.R., 2020. chromoMap: An R package for Interactive Visualization and Annotation of Chromosomes. bioRxiv 605600. https://doi.org/10.1101/605600

Banerjee, A.K., Lin, T., Hannapel, D.J., 2009. Untranslated Regions of a Mobile Transcript Mediate RNA Metabolism. Plant Physiol. 151, 1831–1843. https://doi.org/10.1104/pp.109.144428

Bolger, A.M., Lohse, M., Usadel, B., 2014. Trimmomatic: a flexible trimmer for Illumina sequence data. Bioinformatics 30, 2114–2120. https://doi.org/10.1093/bioinformatics/btu170

Broughton, W.J., Dilworth, M.J., 1971. Control of leghaemoglobin synthesis in snake beans. Biochem. J. 125, 1075–1080.

Buhtz, A., Pieritz, J., Springer, F., Kehr, J., 2010. Phloem small RNAs, nutrient stress responses, and systemic mobility. BMC Plant Biol. 10, 64. https://doi.org/10.1186/1471-2229-10-64

Caetano-Anollés, G., Gresshoff, P.M., 1991. Plant Genetic Control of Nodulation. Annu. Rev. Microbiol. 45, 345–382. https://doi.org/10.1146/annurev.mi.45.100191.002021

Camacho, C., Coulouris, G., Avagyan, V., Ma, N., Papadopoulos, J., Bealer, K., Madden, T.L., 2009. BLAST+: architecture and applications. BMC Bioinformatics 10, 421. https://doi.org/10.1186/1471-2105-10-421

Capella-Gutiérrez, S., Silla-Martínez, J.M., Gabaldón, T., 2009. trimAl: a tool for automated alignment trimming in large-scale phylogenetic analyses. Bioinformatics 25, 1972–1973. https://doi.org/10.1093/bioinformatics/btp348

Carlsbecker, A., Lee, J.-Y., Roberts, C.J., Dettmer, J., Lehesranta, S., Zhou, J., Lindgren, O., Moreno-Risueno, M.A., Vatén, A., Thitamadee, S., Campilho, A., Sebastian, J., Bowman, J.L., Helariutta, Y., Benfey, P.N., 2010. Cell signalling by microRNA165/6 directs gene dose-dependent root cell fate. Nature 465, 316–321. https://doi.org/10.1038/nature08977

Chen, J.G., Crooks, R.M., Seefeldt, L.C., Bren, K.L., Bullock, R.M., Darensbourg, M.Y., Holland, P.L., Hoffman, B., Janik, M.J., Jones, A.K., Kanatzidis, M.G., King, P., Lancaster, K.M., Lymar, S.V., Pfromm, P., Schneider, W.F., Schrock, R.R., 2018. Beyond Fossil-Fuel-Driven Nitrogen Transformations. Science 360. https://doi.org/10.1126/science.aar6611

Chen, X., Yao, Q., Gao, X., Jiang, C., Harberd, N.P., Fu, X., 2016. Shoot-to-Root Mobile Transcription Factor HY5 Coordinates Plant Carbon and Nitrogen Acquisition. Curr. Biol. 26, 640–646. https://doi.org/10.1016/j.cub.2015.12.066

Curtis, M.D., Grossniklaus, U., 2003. A Gateway Cloning Vector Set for High-Throughput Functional Analysis of Genes in Planta. Plant Physiol. 133, 462–469. https://doi.org/10.1104/pp.103.027979

del Campo, E.M., 2009. Post-Transcriptional Control of Chloroplast Gene Expression. Gene Regul. Syst. Biol. 3, 31–47.

Erisman, J.W., Sutton, M.A., Galloway, J., Klimont, Z., Winiwarter, W., 2008. How a century of ammonia synthesis changed the world. Nat. Geosci. 1, 636–639. https://doi.org/10.1038/ngeo325

Food and Agriculture Organization of the United Nations, 2019. World fertilizer trends and outlook to 2022.

Gautrat, P., Laffont, C., Frugier, F., 2020. Compact Root Architecture 2 Promotes Root Competence for Nodulation through the miR2111 Systemic Effector. Curr. Biol. https://doi.org/10.1016/j.cub.2020.01.084

Gautrat, P., Mortier, V., Laffont, C., De Keyser, A., Fromentin, J., Frugier, F., Goormachtig,

S., 2019. Unraveling new molecular players involved in the autoregulation of nodulation in Medicago truncatula. J. Exp. Bot. 70, 1407–1417. https://doi.org/10.1093/jxb/ery465
Herridge, D.F., Peoples, M.B., Boddey, R.M., 2008. Global inputs of biological nitrogen fixation in agricultural systems. Plant Soil 311, 1–18. https://doi.org/10.1007/s11104-008-9668-3
Horchani, F., Hajri, R., Aschi-Smiti, S., 2010. Effect of ammonium or nitrate nutrition on photosynthesis, growth, and nitrogen assimilation in tomato plants. J. Plant Nutr. Soil Sci. 173, 610–617. https://doi.org/10.1002/jpln.201000055
Huen, A., Bally, J., Smith, P., 2018. Identification and characterisation of microRNAs and their target genes in phosphate-starved Nicotiana benthamiana by small RNA deep sequencing and 5'RACE analysis. BMC Genomics 19, 940. https://doi.org/10.1186/s12864-018-5258-9
Ito, S., Kato, T., Ohtake, N., Sueyoshi, K., Ohyama, T., 2008. The Autoregulation of Nodulation Mechanism is Related to Leaf Development. Plant Cell Physiol. 49, 121–125. https://doi.org/10.1093/pcp/pcm161
Jiang, D., Yin, C., Yu, A., Zhou, X., Liang, W., Yuan, Z., Xu, Y., Yu, Q., Wen, T., Zhang, D., 2006. Duplication and expression analysis of multicopy miRNA gene family members in Arabidopsis and rice. Cell Res. 16, 507–518. https://doi.org/10.1038/sj.cr.7310062
Kamal, N., Mun, T., Reid, D., Lin, J.-S., Akyol, T.Y., Sandal, N., Asp, T., Hirakawa, H., Stougaard, J., Mayer, K.F.X., Sato, S., Andersen, S.U., 2020. Insights into the evolution of symbiosis gene copy number and distribution from a chromosome-scale Lotus japonicus Gifu genome sequence. DNA Res. 27. https://doi.org/10.1093/dnares/dsaa015
Karlo, M., Boschiero, C., Landerslev, K.G., Blanco, G.S., Wen, J., Mysore, K.S., Dai, X., Zhao, P.X., de Bang, T.C., 2020. The CLE53–SUNN genetic pathway negatively regulates arbuscular mycorrhiza root colonization in Medicago truncatula. J. Exp. Bot. 71, 4972–4984. https://doi.org/10.1093/jxb/eraa193
Kassaw, T., Nowak, S., Schnabel, E., Frugoli, J., 2017. ROOT DETERMINED NODULATION1 Is Required for M. truncatula CLE12, But Not CLE13, Peptide Signaling through the SUNN Receptor Kinase. Plant Physiol. 174, 2445–2456. https://doi.org/10.1104/pp.17.00278
Katoh, K., Misawa, K., Kuma, K., Miyata, T., 2002. MAFFT: a novel method for rapid multiple sequence alignment based on fast Fourier transform. Nucleic Acids Res. 30, 3059–3066. https://doi.org/10.1093/nar/gkf436
Kawaguchi, M., 2000. Lotus japonicus `Miyakojima' MG-20: An Early-Flowering Accession Suitable for Indoor Handling. J. Plant Res. 113, 507–509. https://doi.org/10.1007/PL00013961
Kim, B., Arcos, S., Rothamel, K., Jian, J., Rose, K.L., McDonald, W.H., Bian, Y., Reasoner, S., Barrows, N.J., Bradrick, S., Garcia-Blanco, M.A., Ascano, M., 2020. Discovery of Widespread Host Protein Interactions with the Pre-replicated Genome of CHIKV Using VIR-CLASP. Mol. Cell 78, 624-640.e7. https://doi.org/10.1016/j.molcel.2020.04.013
Kim, D., Paggi, J.M., Park, C., Bennett, C., Salzberg, S.L., 2019. Graph-based genome alignment and genotyping with HISAT2 and HISAT-genotype. Nat. Biotechnol. 37, 907–915. https://doi.org/10.1038/s41587-019-0201-4
Ko, D., Helariutta, Y., 2017. Shoot–Root Communication in Flowering Plants. Curr. Biol. 27, R973–R978. https://doi.org/10.1016/j.cub.2017.06.054
Kozomara, A., Griffiths-Jones, S., 2011. miRBase: integrating microRNA annotation and

deep-sequencing data. Nucleic Acids Res. 39, D152–D157. https://doi.org/10.1093/nar/gkq1027
Krusell, L., Madsen, L.H., Sato, S., Aubert, G., Genua, A., Szczyglowski, K., Duc, G., Kaneko, T., Tabata, S., Bruijn, F. de, Pajuelo, E., Sandal, N., Stougaard, J., 2002. Shoot control of root development and nodulation is mediated by a receptor-like kinase. Nature 420, 422–426. https://doi.org/10.1038/nature01207
Landrein, B., Formosa-Jordan, P., Malivert, A., Schuster, C., Melnyk, C.W., Yang, W., Turnbull, C., Meyerowitz, E.M., Locke, J.C.W., Jönsson, H., 2018. Nitrate modulates stem cell dynamics in Arabidopsis shoot meristems through cytokinins. Proc. Natl. Acad. Sci. U. S. A. 115, 1382–1387. https://doi.org/10.1073/pnas.1718670115
Ledgard, S.F., Sprosen, M.S., Steele, K.W., 1996. Nitrogen fixation by nine white clover cultivars in grazed pasture, as affected by nitrogen fertilization. Plant Soil 178, 193–203. https://doi.org/10.1007/BF00011583
Li, A., Mao, L., 2007. Evolution of plant microRNA gene families. Cell Res. 17, 212–218. https://doi.org/10.1038/sj.cr.7310113
Li, H., Handsaker, B., Wysoker, A., Fennell, T., Ruan, J., Homer, N., Marth, G., Abecasis, G., Durbin, R., 2009. The Sequence Alignment/Map format and SAMtools. Bioinformatics 25, 2078–2079. https://doi.org/10.1093/bioinformatics/btp352
Liang, G., Ai, Q., Yu, D., 2015. Uncovering miRNAs involved in crosstalk between nutrient deficiencies in Arabidopsis. Sci. Rep. 5, 1–13. https://doi.org/10.1038/srep11813
Lin, S.-I., Chiang, S.-F., Lin, W.-Y., Chen, J.-W., Tseng, C.-Y., Wu, P.-C., Chiou, T.-J., 2008. Regulatory Network of MicroRNA399 and PHO2 by Systemic Signaling. Plant Physiol. 147, 732–746. https://doi.org/10.1104/pp.108.116269
Liu, H., Ding, Y., Zhou, Y., Jin, W., Xie, K., Chen, L.-L., 2017. CRISPR-P 2.0: An Improved CRISPR-Cas9 Tool for Genome Editing in Plants. Mol. Plant 10, 530–532. https://doi.org/10.1016/j.molp.2017.01.003
Ma, D., Endo, S., Betsuyaku, S., Shimotohno, A., Fukuda, H., 2020. CLE2 regulates light-dependent carbohydrate metabolism in Arabidopsis shoots. Plant Mol. Biol. 104, 561–574. https://doi.org/10.1007/s11103-020-01059-y
Maekawa, T., Kusakabe, M., Shimoda, Y., Sato, S., Tabata, S., Murooka, Y., Hayashi, M., 2008. Polyubiquitin promoter-based binary vectors for overexpression and gene silencing in Lotus japonicus. Mol. Plant-Microbe Interact. MPMI 21, 375–382. https://doi.org/10.1094/MPMI-21-4-0375
Magori, S., Oka-Kira, E., Shibata, S., Umehara, Y., Kouchi, H., Hase, Y., Tanaka, A., Sato, S., Tabata, S., Kawaguchi, M., 2009. TOO MUCH LOVE, a Root Regulator Associated with the Long-Distance Control of Nodulation in Lotus japonicus. Mol. Plant-Microbe Interact. MPMI 22, 259–268. https://doi.org/10.1094/MPMI-22-3-0259
Maher, C., Stein, L., Ware, D., 2006. Evolution of Arabidopsis microRNA families through duplication events. Genome Res. 16, 510–519. https://doi.org/10.1101/gr.4680506
Markmann, K., Parniske, M., 2009. Evolution of root endosymbiosis with bacteria: how novel are nodules? Trends Plant Sci. 14, 77–86. https://doi.org/10.1016/j.tplants.2008.11.009
Masclaux-Daubresse, C., Daniel-Vedele, F., Dechorgnat, J., Chardon, F., Gaufichon, L., Suzuki, A., 2010. Nitrogen uptake, assimilation and remobilization in plants: challenges for sustainable and productive agriculture. Ann. Bot. 105, 1141–1157. https://doi.org/10.1093/aob/mcq028
Mateos, J.L., Bologna, N.G., Chorostecki, U., Palatnik, J.F., 2010. Identification of MicroRNA Processing Determinants by Random Mutagenesis of Arabidopsis MIR172a Precursor. Curr. Biol. 20, 49–54. https://doi.org/10.1016/j.cub.2009.10.072
Miyashima, S., Honda, M., Hashimoto, K., Tatematsu, K., Hashimoto, T., Sato-Nara, K.,

Okada, K., Nakajima, K., 2013. A Comprehensive Expression Analysis of the Arabidopsis MICRORNA165/6 Gene Family during Embryogenesis Reveals a Conserved Role in Meristem Specification and a Non-Cell-Autonomous Function. Plant Cell Physiol. 54, 375–384. https://doi.org/10.1093/pcp/pcs188

Moro, B., Chorostecki, U., Arikit, S., Suarez, I.P., Höbartner, C., Rasia, R.M., Meyers, B.C., Palatnik, J.F., 2018. Efficiency and precision of microRNA biogenesis modes in plants. Nucleic Acids Res. 46, 10709–10723. https://doi.org/10.1093/nar/gky853

Mortier, V., Herder, G.D., Whitford, R., Velde, W.V. de, Rombauts, S., D'haeseleer, K., Holsters, M., Goormachtig, S., 2010. CLE Peptides Control Medicago truncatula Nodulation Locally and Systemically. Plant Physiol. 153, 222–237. https://doi.org/10.1104/pp.110.153718

Müller, L.M., Flokova, K., Schnabel, E., Sun, X., Fei, Z., Frugoli, J., Bouwmeester, H.J., Harrison, M.J., 2019. A CLE–SUNN module regulates strigolactone content and fungal colonization in arbuscular mycorrhiza. Nat. Plants 5, 933–939. https://doi.org/10.1038/s41477-019-0501-1

Nagae, M., Parniske, M., Kawaguchi, M., Takeda, N., 2016. The Thiamine Biosynthesis Gene THI1 Promotes Nodule Growth and Seed Maturation. Plant Physiol. 172, 2033–2043. https://doi.org/10.1104/pp.16.01254

Nguyen, L.-T., Schmidt, H.A., von Haeseler, A., Minh, B.Q., 2015. IQ-TREE: A Fast and Effective Stochastic Algorithm for Estimating Maximum-Likelihood Phylogenies. Mol. Biol. Evol. 32, 268–274. https://doi.org/10.1093/molbev/msu300

Nishida, H., Handa, Y., Tanaka, S., Suzaki, T., Kawaguchi, M., 2016. Expression of the CLE-RS3 gene suppresses root nodulation in Lotus japonicus. J. Plant Res. 129, 909–919. https://doi.org/10.1007/s10265-016-0842-z

Nishida, H., Tanaka, S., Handa, Y., Ito, M., Sakamoto, Y., Matsunaga, S., Betsuyaku, S., Miura, K., Soyano, T., Kawaguchi, M., Suzaki, T., 2018. A NIN-LIKE PROTEIN mediates nitrate-induced control of root nodule symbiosis in Lotus japonicus. Nat. Commun. 9, 499. https://doi.org/10.1038/s41467-018-02831-x

Nishimura, R., Hayashi, M., Wu, G.-J., Kouchi, H., Imaizumi-Anraku, H., Murakami, Y., Kawasaki, S., Akao, S., Ohmori, M., Nagasawa, M., Harada, K., Kawaguchi, M., 2002. HAR1 mediates systemic regulation of symbiotic organ development. Nature 420, 426–429. https://doi.org/10.1038/nature01231

Nontachaiyapoom, S., Scott, P.T., Men, A.E., Kinkema, M., Schenk, P.M., Gresshoff, P.M., 2007. Promoters of orthologous Glycine max and Lotus japonicus nodulation autoregulation genes interchangeably drive phloem-specific expression in transgenic plants. Mol. Plant-Microbe Interact. MPMI 20, 769–780. https://doi.org/10.1094/MPMI-20-7-0769

Nunes-Nesi, A., Fernie, A.R., Stitt, M., 2010. Metabolic and Signaling Aspects Underpinning the Regulation of Plant Carbon Nitrogen Interactions. Mol. Plant 3, 973–996. https://doi.org/10.1093/mp/ssq049

Ohkubo, Y., Tanaka, M., Tabata, R., Ogawa-Ohnishi, M., Matsubayashi, Y., 2017. Shoot-to-root mobile polypeptides involved in systemic regulation of nitrogen acquisition. Nat. Plants 3, 17029. https://doi.org/10.1038/nplants.2017.29

Ohyama, T., 2017. The Role of Legume-Rhizobium Symbiosis in Sustainable Agriculture, in: Sulieman, S., Tran, L.-S.P. (Eds.), Legume Nitrogen Fixation in Soils with Low Phosphorus Availability: Adaptation and Regulatory Implication. Springer International Publishing, Cham, pp. 1–20. https://doi.org/10.1007/978-3-319-55729-8_1

Okamoto, S., Ohnishi, E., Sato, S., Takahashi, H., Nakazono, M., Tabata, S., Kawaguchi, M., 2009. Nod Factor/Nitrate-Induced CLE Genes that Drive HAR1-Mediated Systemic

Regulation of Nodulation. Plant Cell Physiol. 50, 67–77. https://doi.org/10.1093/pcp/pcn194
Okamoto, S., Shinohara, H., Mori, T., Matsubayashi, Y., Kawaguchi, M., 2013a. Root-derived CLE glycopeptides control nodulation by direct binding to HAR1 receptor kinase. Nat. Commun. 4, 2191. https://doi.org/10.1038/ncomms3191
Okamoto, S., Shinohara, H., Mori, T., Matsubayashi, Y., Kawaguchi, M., 2013b. Root-derived CLE glycopeptides control nodulation by direct binding to HAR1 receptor kinase. Nat. Commun. 4, 1–7. https://doi.org/10.1038/ncomms3191
Okuma, N., Soyano, T., Suzaki, T., Kawaguchi, M., 2020. MIR2111-5 locus and shoot-accumulated mature miR2111 systemically enhance nodulation depending on HAR1 in Lotus japonicus. Nat. Commun. 11, 5192. https://doi.org/10.1038/s41467-020-19037-9
Oldroyd, G.E.D., Leyser, O., 2020. A plant's diet, surviving in a variable nutrient environment. Science 368. https://doi.org/10.1126/science.aba0196
Ota, R., Ohkubo, Y., Yamashita, Y., Ogawa-Ohnishi, M., Matsubayashi, Y., 2020. Shoot-to-root mobile CEPD-like 2 integrates shoot nitrogen status to systemically regulate nitrate uptake in Arabidopsis. Nat. Commun. 11, 641. https://doi.org/10.1038/s41467-020-14440-8
Pagliarani, C., Gambino, G., 2019. Small RNA Mobility: Spread of RNA Silencing Effectors and its Effect on Developmental Processes and Stress Adaptation in Plants. Int. J. Mol. Sci. 20. https://doi.org/10.3390/ijms20174306
Pant, B.D., Buhtz, A., Kehr, J., Scheible, W.-R., 2008. MicroRNA399 is a long-distance signal for the regulation of plant phosphate homeostasis. Plant J. 53, 731–738. https://doi.org/10.1111/j.1365-313X.2007.03363.x
Pant, B.D., Musialak-Lange, M., Nuc, P., May, P., Buhtz, A., Kehr, J., Walther, D., Scheible, W.-R., 2009. Identification of Nutrient-Responsive Arabidopsis and Rapeseed MicroRNAs by Comprehensive Real-Time Polymerase Chain Reaction Profiling and Small RNA Sequencing. Plant Physiol. 150, 1541–1555. https://doi.org/10.1104/pp.109.139139
Pertea, M., Pertea, G.M., Antonescu, C.M., Chang, T.-C., Mendell, J.T., Salzberg, S.L., 2015. StringTie enables improved reconstruction of a transcriptome from RNA-seq reads. Nat. Biotechnol. 33, 290–295. https://doi.org/10.1038/nbt.3122
Poitout, A., Crabos, A., Petřík, I., Novák, O., Krouk, G., Lacombe, B., Ruffel, S., 2018. Responses to Systemic Nitrogen Signaling in Arabidopsis Roots Involve trans-Zeatin in Shoots. Plant Cell 30, 1243–1257. https://doi.org/10.1105/tpc.18.00011
Ramírez, F., Ryan, D.P., Grüning, B., Bhardwaj, V., Kilpert, F., Richter, A.S., Heyne, S., Dündar, F., Manke, T., 2016. deepTools2: a next generation web server for deep-sequencing data analysis. Nucleic Acids Res. 44, W160–W165. https://doi.org/10.1093/nar/gkw257
Reid, D.E., Ferguson, B.J., Gresshoff, P.M., 2011a. Inoculation- and Nitrate-Induced CLE Peptides of Soybean Control NARK-Dependent Nodule Formation. Mol. Plant-Microbe Interact. MPMI 24, 606–618. https://doi.org/10.1094/MPMI-09-10-0207
Reid, D.E., Ferguson, B.J., Hayashi, S., Lin, Y.-H., Gresshoff, P.M., 2011b. Molecular mechanisms controlling legume autoregulation of nodulation. Ann. Bot. 108, 789–795. https://doi.org/10.1093/aob/mcr205
Reid, D.E., Li, D., Ferguson, B.J., Gresshoff, P.M., 2013. Structure–function analysis of the GmRIC1 signal peptide and CLE domain required for nodulation control in soybean. J. Exp. Bot. 64, 1575–1585. https://doi.org/10.1093/jxb/ert008
Reuter, J.S., Mathews, D.H., 2010. RNAstructure: software for RNA secondary structure prediction and analysis. BMC Bioinformatics 11, 129. https://doi.org/10.1186/1471-

2105-11-129
Ritter, A., Iñigo, S., Fernández-Calvo, P., Heyndrickx, K.S., Dhondt, S., Shi, H., De Milde, L., Vanden Bossche, R., De Clercq, R., Eeckhout, D., Ron, M., Somers, D.E., Inzé, D., Gevaert, K., De Jaeger, G., Vandepoele, K., Pauwels, L., Goossens, A., 2017. The transcriptional repressor complex FRS7-FRS12 regulates flowering time and growth in Arabidopsis. Nat. Commun. 8, 15235. https://doi.org/10.1038/ncomms15235
Robinson, J.T., Thorvaldsdóttir, H., Winckler, W., Guttman, M., Lander, E.S., Getz, G., Mesirov, J.P., 2011. Integrative genomics viewer. Nat. Biotechnol. 29, 24–26. https://doi.org/10.1038/nbt.1754
Roy, S., Liu, W., Nandety, R.S., Crook, A., Mysore, K.S., Pislariu, C.I., Frugoli, J., Dickstein, R., Udvardi, M.K., 2020. Celebrating 20 Years of Genetic Discoveries in Legume Nodulation and Symbiotic Nitrogen Fixation. Plant Cell 32, 15–41. https://doi.org/10.1105/tpc.19.00279
Sasaki, T., Suzaki, T., Soyano, T., Kojima, M., Sakakibara, H., Kawaguchi, M., 2014. Shoot-derived cytokinins systemically regulate root nodulation. Nat. Commun. 5, 4983. https://doi.org/10.1038/ncomms5983
Scheible, W.-R., Morcuende, R., Czechowski, T., Fritz, C., Osuna, D., Palacios-Rojas, N., Schindelasch, D., Thimm, O., Udvardi, M.K., Stitt, M., 2004. Genome-Wide Reprogramming of Primary and Secondary Metabolism, Protein Synthesis, Cellular Growth Processes, and the Regulatory Infrastructure of Arabidopsis in Response to Nitrogen. Plant Physiol. 136, 2483–2499. https://doi.org/10.1104/pp.104.047019
Schnabel, E., Journet, E.-P., de Carvalho-Niebel, F., Duc, G., Frugoli, J., 2005. The Medicago truncatula SUNN Gene Encodes a CLV1-likeLeucine-rich Repeat Receptor Kinase that Regulates Nodule Number and Root Length. Plant Mol. Biol. 58, 809–822. https://doi.org/10.1007/s11103-005-8102-y
Schnabel, E.L., Kassaw, T.K., Smith, L.S., Marsh, J.F., Oldroyd, G.E., Long, S.R., Frugoli, J.A., 2011. The ROOT DETERMINED NODULATION1 Gene Regulates Nodule Number in Roots of Medicago truncatula and Defines a Highly Conserved, Uncharacterized Plant Gene Family. Plant Physiol. 157, 328–340. https://doi.org/10.1104/pp.111.178756
Searle, I.R., Men, A.E., Laniya, T.S., Buzas, D.M., Iturbe-Ormaetxe, I., Carroll, B.J., Gresshoff, P.M., 2003. Long-Distance Signaling in Nodulation Directed by a CLAVATA1-Like Receptor Kinase. Science 299, 109–112. https://doi.org/10.1126/science.1077937
Shao, C.-H., Qiu, C.-F., Qian, Y.-F., Liu, G.-R., 2020. Nitrate deficiency decreased photosynthesis and oxidation-reduction processes, but increased cellular transport, lignin biosynthesis and flavonoid metabolism revealed by RNA-Seq in Oryza sativa leaves. PLOS ONE 15, e0235975. https://doi.org/10.1371/journal.pone.0235975
Suzaki, T., Yoro, E., Kawaguchi, M., 2015. Chapter Three - Leguminous Plants: Inventors of Root Nodules to Accommodate Symbiotic Bacteria, in: Jeon, K.W. (Ed.), International Review of Cell and Molecular Biology. Academic Press, pp. 111–158. https://doi.org/10.1016/bs.ircmb.2015.01.004
Tabata, R., Sumida, K., Yoshii, T., Ohyama, K., Shinohara, H., Matsubayashi, Y., 2014. Perception of root-derived peptides by shoot LRR-RKs mediates systemic N-demand signaling. Science 346, 343–346. https://doi.org/10.1126/science.1257800
Takahara, M., Magori, S., Soyano, T., Okamoto, S., Yoshida, C., Yano, K., Sato, S., Tabata, S., Yamaguchi, K., Shigenobu, S., Takeda, N., Suzaki, T., Kawaguchi, M., 2013. TOO MUCH LOVE, a Novel Kelch Repeat-Containing F-box Protein, Functions in the Long-Distance Regulation of the Legume–Rhizobium Symbiosis. Plant Cell Physiol. 54, 433–447. https://doi.org/10.1093/pcp/pct022

Tanabata S., Ohtake N., Sueyoshi K., Kawaguchi M., Ohyama T., 2013. Leaf growth of Lotus japonicus hypernodulation mutant har1-4. Bull. Fac. Agric. Niigata Univ. 66, 21–24.

Tatematsu, K., Toyokura, K., Miyashima, S., Nakajima, K., Okada, K., 2015. A molecular mechanism that confines the activity pattern of miR165 in Arabidopsis leaf primordia. Plant J. 82, 596–608. https://doi.org/10.1111/tpj.12834

Tsai, Y.-C., Chen, K.-C., Cheng, T.-S., Lee, C., Lin, S.-H., Tung, C.-W., 2019. Chlorophyll fluorescence analysis in diverse rice varieties reveals the positive correlation between the seedlings salt tolerance and photosynthetic efficiency. BMC Plant Biol. 19, 403. https://doi.org/10.1186/s12870-019-1983-8

Tsikou, D., Yan, Z., Holt, D.B., Abel, N.B., Reid, D.E., Madsen, L.H., Bhasin, H., Sexauer, M., Stougaard, J., Markmann, K., 2018. Systemic control of legume susceptibility to rhizobial infection by a mobile microRNA. Science 362, 233–236. https://doi.org/10.1126/science.aat6907

Vinther, F.P., 1998. Biological nitrogen fixation in grass–clover affected by animal excreta. Plant Soil 203, 207–215. https://doi.org/10.1023/A:1004378913380

Werner, S., Wollmann, H., Schneeberger, K., Weigel, D., 2010. Structure Determinants for Accurate Processing of miR172a in Arabidopsis thaliana. Curr. Biol. 20, 42–48. https://doi.org/10.1016/j.cub.2009.10.073

Wopereis, J., Pajuelo, E., Dazzo, F.B., Jiang, Q., Gresshoff, P.M., Bruijn, F.J.D., Stougaard, J., Szczyglowski, K., 2000. Short root mutant of Lotus japonicus with a dramatically altered symbiotic phenotype. Plant J. 23, 97–114. https://doi.org/10.1046/j.1365-313x.2000.00799.x

Yan, J., Gu, Y., Jia, X., Kang, W., Pan, S., Tang, X., Chen, X., Tang, G., 2012. Effective Small RNA Destruction by the Expression of a Short Tandem Target Mimic in Arabidopsis. Plant Cell 24, 415–427. https://doi.org/10.1105/tpc.111.094144

Yoro, E., Nishida, H., Ogawa-Ohnishi, M., Yoshida, C., Suzaki, T., Matsubayashi, Y., Kawaguchi, M., 2019. PLENTY, a hydroxyproline O-arabinosyltransferase, negatively regulates root nodule symbiosis in Lotus japonicus. J. Exp. Bot. 70, 507–517. https://doi.org/10.1093/jxb/ery364

Yu, G., Smith, D.K., Zhu, H., Guan, Y., Lam, T.T.-Y., 2017. ggtree: an r package for visualization and annotation of phylogenetic trees with their covariates and other associated data. Methods Ecol. Evol. 8, 28–36. https://doi.org/10.1111/2041-210X.12628

Zhang, M., Su, H., Gresshoff, P.M., Ferguson, B.J., 2021. Shoot-derived miR2111 controls legume root and nodule development. Plant Cell Environ. https://doi.org/10.1111/pce.13992

Zhang, X., Davidson, E.A., Mauzerall, D.L., Searchinger, T.D., Dumas, P., Shen, Y., 2015. Managing nitrogen for sustainable development. Nature 528, 51–59. https://doi.org/10.1038/nature15743

Acknowledgments

I express my sincere thanks to Dr. Masayoshi Kawaguchi for his great supervision and Dr. Takashi Soyano for his helpful advice. Without their guidance, my dissertation would not have been possible.

I would like to thank the Life Science Progress Committee, Dr. Shuji Shigenobu, Dr. Kazuhiro Aoki, Dr. Akira Yamashita, and Dr. Kensuke Kawade.

Also, I was supported by collaborators. I thank Dr. Takuya Suzaki (Tsukuba University) for his critical suggestion and technical advice; Dr. Shusei Sato (Tohoku University) for sharing unpublished *L. japonicus* genomic assembly (Gifu v1.2) and for his critical suggestions with the identification of *L. japonicus* miR2111 genes; Dr. Anne Britt, Dr. Mily Ron (University of California, Davis), Dr. Masaki Endo, and Dr. Seiichi Toki (National Agriculture and Food Research Organization) for providing pMR series vectors; Dr. Kiyoshi Tatematsu (National Institute for Basic Biology, NIBB) for discussions; Dr. Taro Maeda (Ryukoku University) and Dr. Hiromu Kameoka (Tohoku University) for their suggestions with bioinformatic analyses; and Ms. Akiko Oda, Ms. Sachiko Tanaka, Ms. Yuko Ogawa, Ms. Yumi Yoshinori, Ms. Asami Tokairin (NIBB), and Dr. Momoyo Ito (University of Tsukuba) for their experimental support; Functional Genomics Facility (NIBB Core Research Facilities), the Data Integration and Analysis Facility (NIBB), Model Plant Research Facility (NIBB Bioresource Center) for their technical supports.

I would like to offer my special thanks to the current and former lab members for their support. Finally, I want to thank my family.

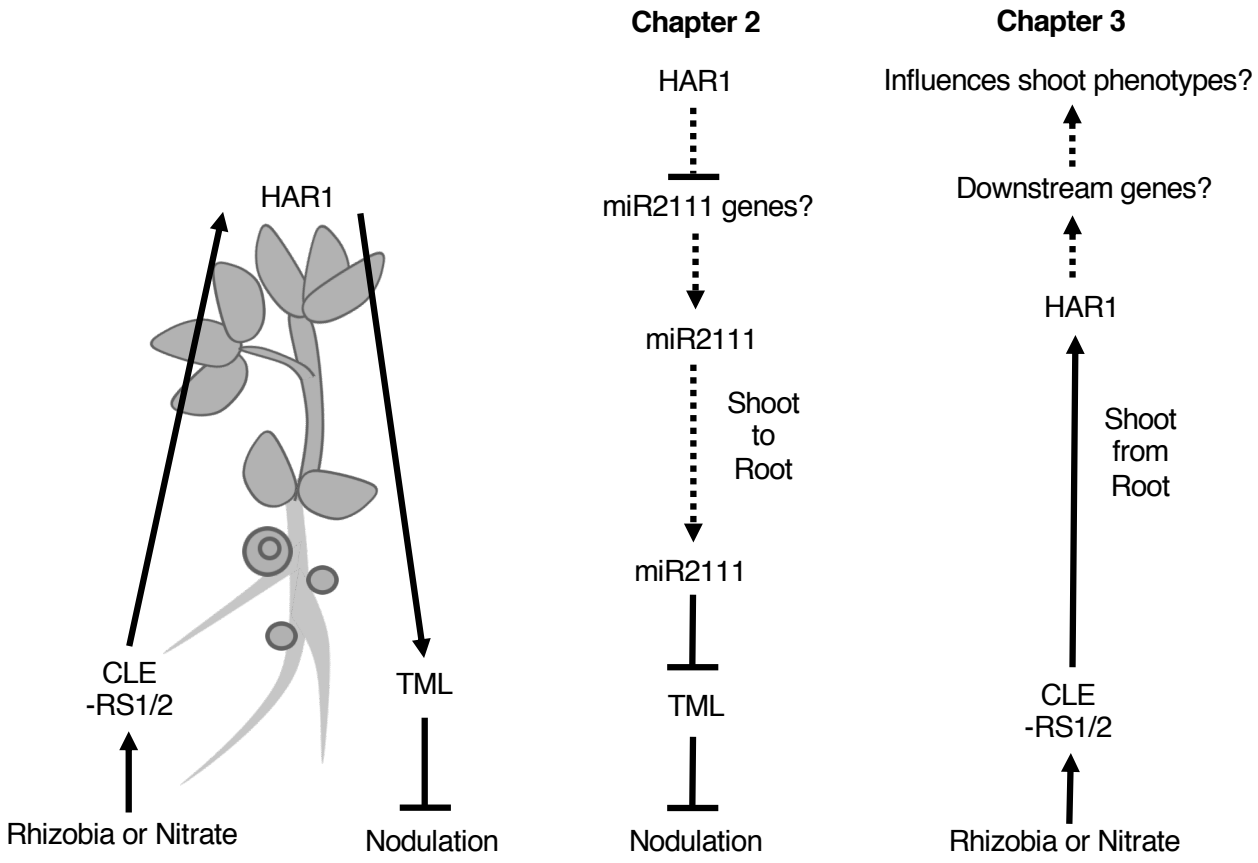

Figure 1.1: Working hypotheses in Chapter 2 and 3

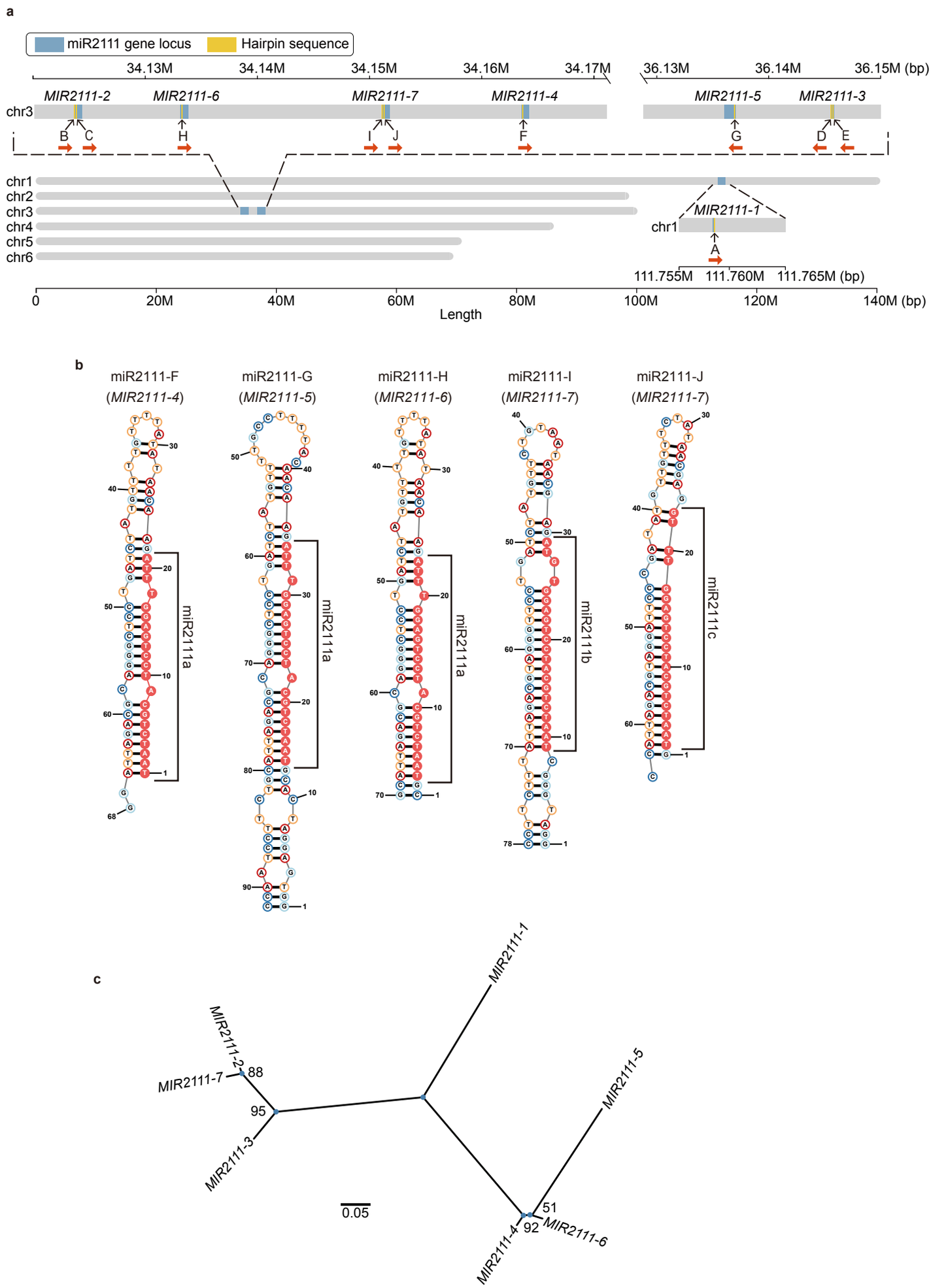

Figure 2.1 Distribution of miR2111 genes on *L. japonicus* genome, secondary structures of news miR2111s, and phylogenetic relationship of miR2111 genes.

Figure 2.1: **Distribution of miR2111 genes on *L. japonicus* genome, secondary structures of news miR2111s, and phylogenetic relationship of miR2111 genes.**
a Distribution of miR2111 genes on *L. japonicus* genome. Blue and yellow boxes indicate the positions of miR2111 genes (*MIR2111-1* to *MIR2111-7*) and miR2111 hairpin sequences (miR2111-A to miR2111-J), respectively. *MIR2111-2*, *MIR2111-3*, and *MIR2111-7* possess two miR2111 hairpin sequences. Red arrows represent the directions of mature miR2111s. **b** Hairpin structures of miR2111-F to miR2111-J. All secondary structures were predicted using the full-length sequence of the predicted miR2111 genes by means of the minimum free energy (MFE) algorithm of RNAstructure software (ver. 6.1). Nucleotides filled with red color indicate mature miR2111 sequences. **c** Maximum likelihood tree of miR2111 genes. Bootstrap values were calculated from 1000 times bootstrap replicates and described at each node. Scale bar represents the branch length.

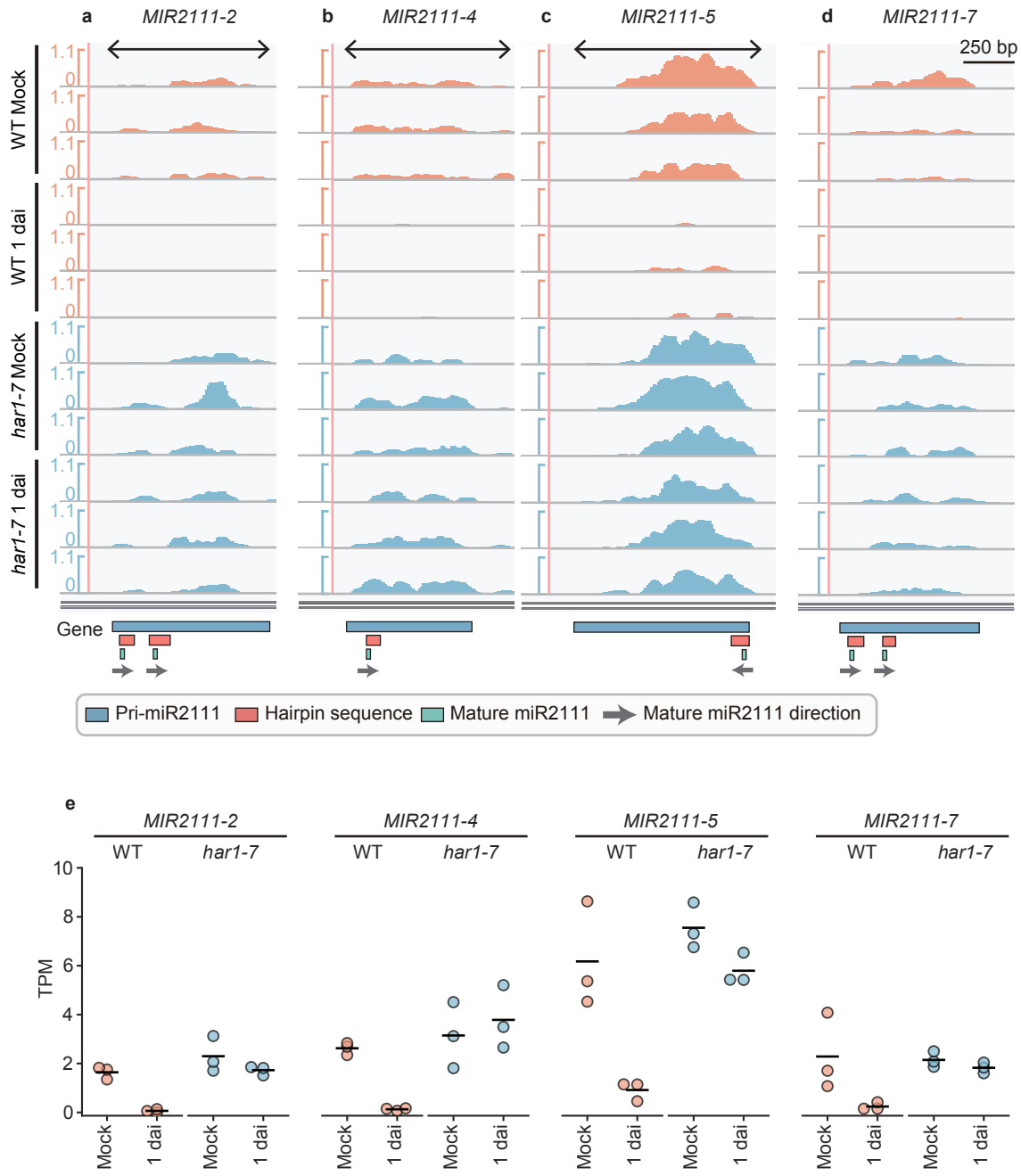

Figure 2.2: Expression of four *L. japonicus* miR2111 genes including those identified by RNA-seq analysis.

Figure 2.2: Expression of four *L. japonicus* miR2111 genes including those identified by RNA-seq analysis.

a-d RNA-seq read coverage of *MIR2111-2* (a), *MIR2111-4* (b), *MIR2111-5* (c), and *MIR2111-7* (d) were visualized by the Integrative Genomics Viewer. All data were acquired by RNA-seq of mature leaves of wild-type (MG-20) and *har1-7* plants that were inoculated with *M. loti* (1 day after inoculation) or mock-treated (control). RNA-seq libraries were prepared using poly(A) enrichment method and miR2111 genes were predicted by RNA-Seq-based gene prediction using Stringtie version 1.3.4d with default settings. Read abundance normalized in bins per million (BPM) is shown. Gray arrows in the gene column represent the directions of mature miR2111 (*Bottom*). Regions used for the overexpression assay are indicated as black two-directional arrows (*Top*) (see Fig. 2.4). **e** Transcripts per million (TPM) values of four miR2111 genes. Scatterplots show individual biological replicates as dots. Bars indicate mean values.

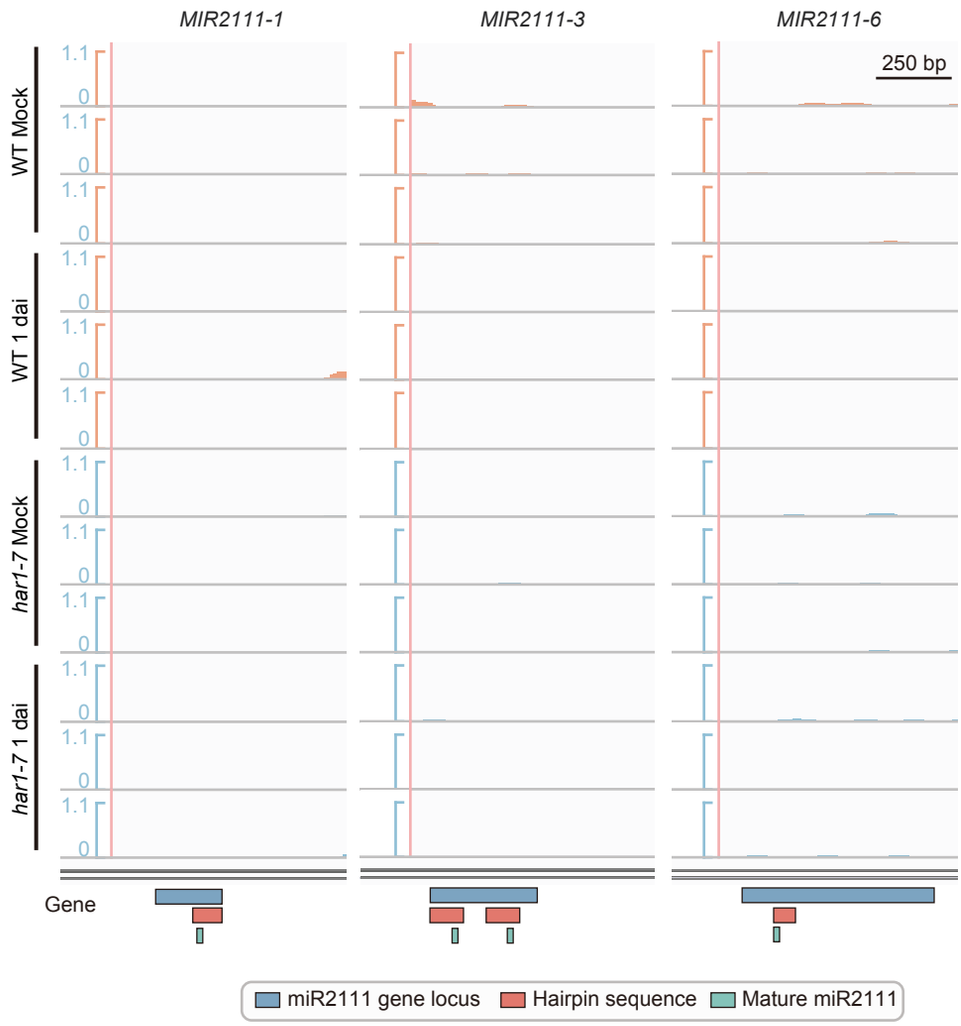

Figure 2.3: RNA-seq read coverage of *MIR2111-1*, *MIR2111-3*, and *MIR2111-6*.

Figure 2.3: **RNA-seq read coverage of *MIR2111-1*, *MIR2111-3*, and *MIR2111-6.***
RNA-seq read coverage of *MIR2111-1*, *MIR2111-3*, and *MIR2111-6*. All data were acquired by RNA-seq of mature leaves of wild-type (MG-20) and *har1-7* plants that were inoculated with *M. loti* (1 day after inoculation) or mock-treated (control). RNA-seq libraries were prepared with poly(A) enrichment methods. miR2111 genes were predicted by RNA-seq alignment assembly using Stringtie version 1.3.4d with default settings. Read abundance normalized in bins per million (BPM) is shown.

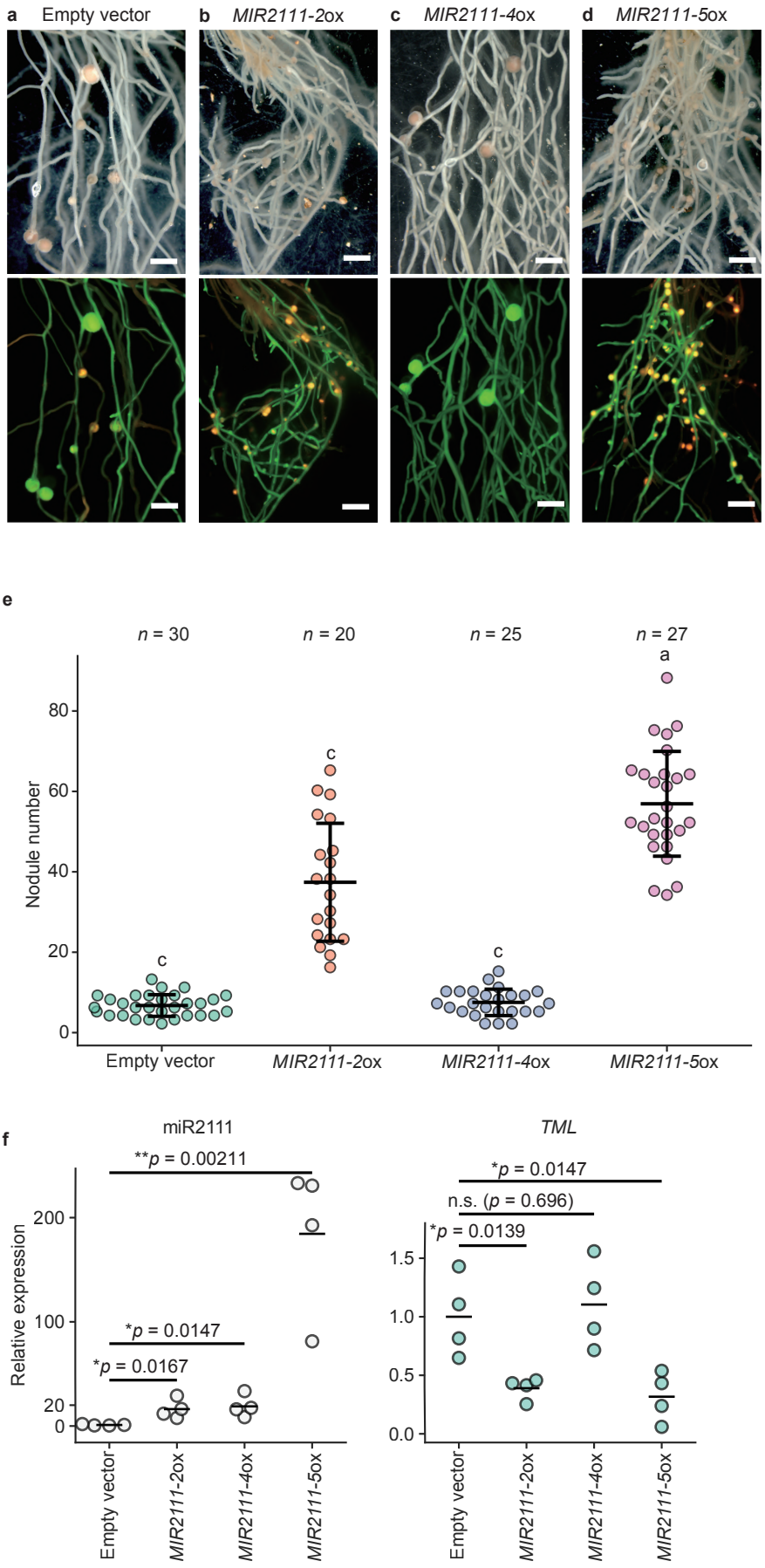

Figure 2.4: Over-expression of *MIR2111-2* and *MIR2111-5* in roots promoted nodulation.

Figure 2.4: Overexpression of *MIR2111-2* and *MIR2111-5* in hairy roots promoted nodulation.

a-d Nodulation at 21 days after inoculation (dai) on hairy roots transformed with an empty vector (a), *proUBQ:MIR2111-2* (b), *proUBQ:MIR2111-4* (c), and *proUBQ:MIR2111-5* (d). Bright images (*Upper*) and corresponding fluorescence images as a GFP transformation marker and DsRed constitutively expressing in *M. loti* (*Lower*). Scale bars: 2 mm. **e** Nodule numbers in hairy roots transformed with an empty vector, *proUBQ:MIR2111-2*, *proUBQ:MIR2111-4*, and *proUBQ1MIR2111-5* (21 dai). Bars indicate mean ± standard deviation. Different letters indicate significant differences ($p < 0.05$) from Tukey's honestly significant difference test. **f** qRT-PCR analyses of mature miR2111 and *TML* in transformed hairy roots (5 dai). $n = 4$ individual biological replicates for each treatment. Bars indicate mean values. (e, f) Scatterplots show individual biological replicates as dots. Two-sided Student's *t*-test was used to determine statistical difference compared with empty vector control: *, $p < 0.05$; **, $p < 0.01$; n.s., not significant.

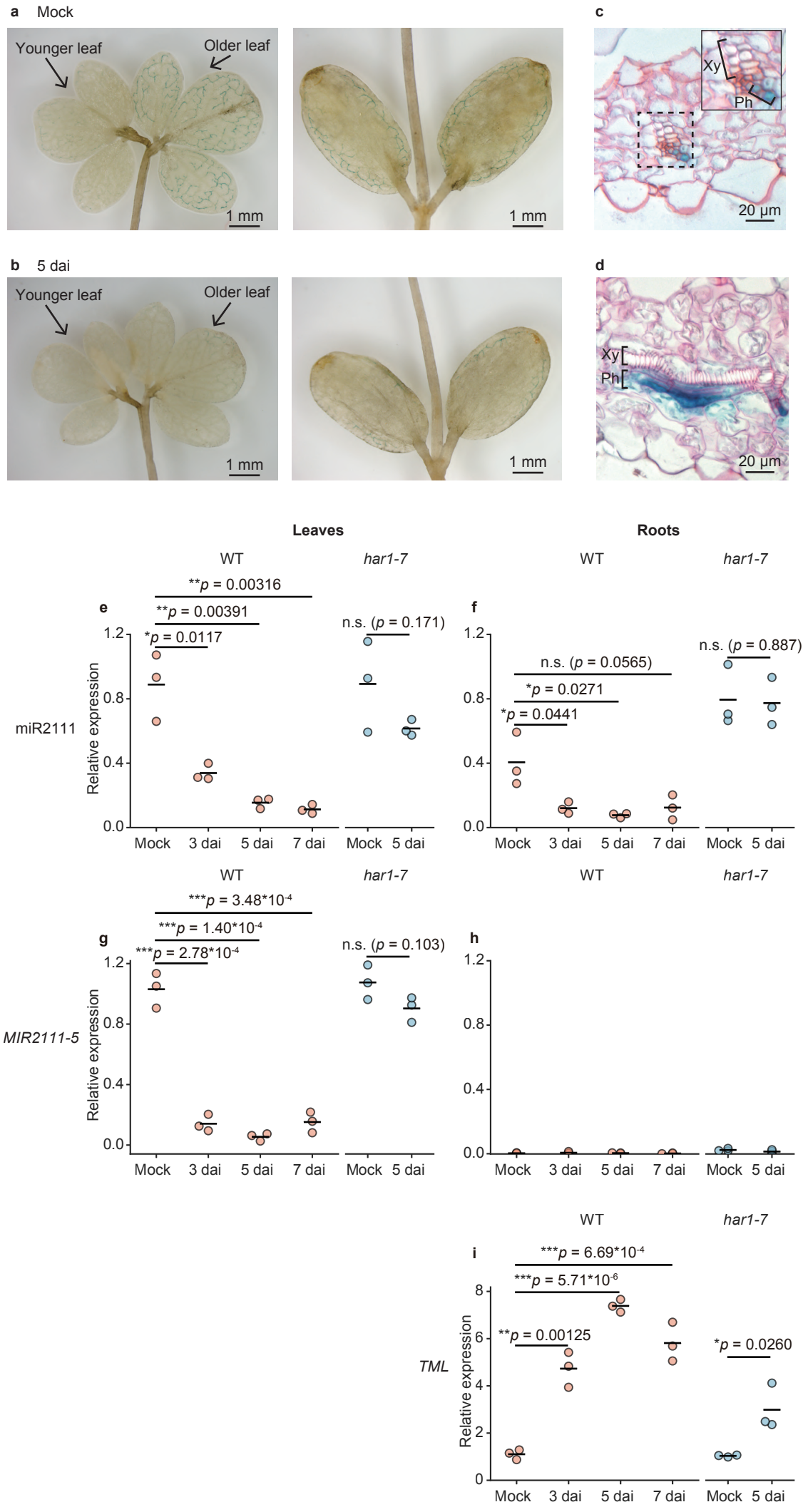

Figure 2.5: *MIR2111-5* was expressed mainly in the phloem of mature leaves.

Figure 2.5: *MIR2111-5* was expressed mainly in the phloem of mature leaves.
a-d GUS expression controlled by a 3.0 kb DNA fragment upstream of *MIR2111-5* in true leaves (*Left*) and cotyledon (*Right*) of plants mock-treated (a, c, d) and inoculated with *M. loti* (5 days after inoculation) (b) were incubated in GUS staining buffer for 3 h. (c, d) Leaf sections counterstained with 0.1% safranin for 10 minutes. Xy: xylem; Ph: phloem. **e-h** qRT-PCR analyses of mature miR2111s (e, f) and *MIR2111-5* (f, g), and *TML* (i) in leaves (e, g) and roots (f, h, i) at indicated days after inoculation (dai) with *M. loti.* Scatterplots show individual biological replicates as dots. Bars indicate mean values. All values were normalized by the mean value of wild-type mock-treated leaves. Two-sided Student's *t*-test was used to determine statistical difference compared with mock control: *, $p < 0.05$; **, $p < 0.01$; ***, $p < 0.001$; n.s., not significant.

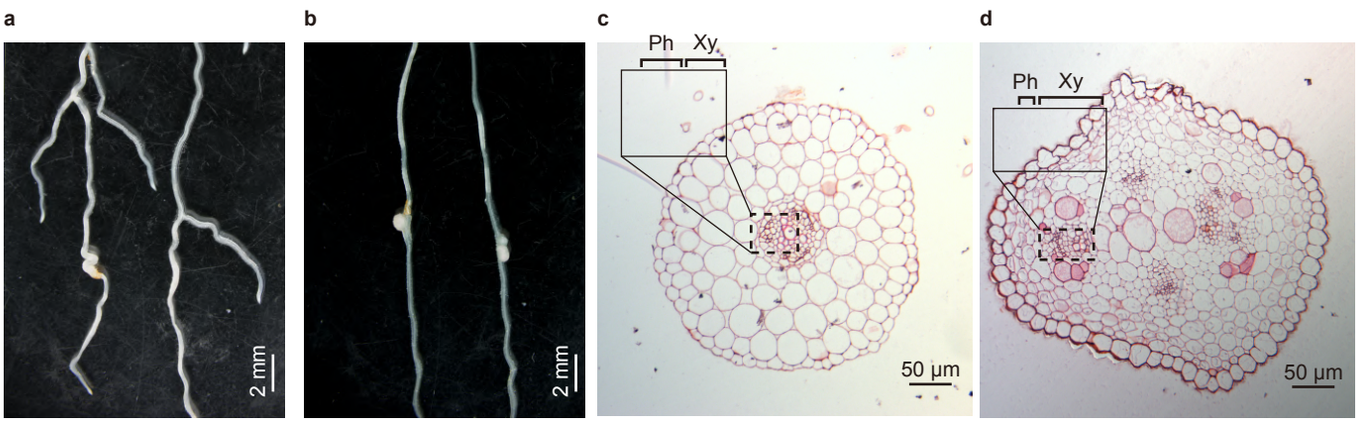

Figure 2.6: *MIR2111-5* was expressed neither in roots, root nodules, nor stems.

Figure 2.6: ***MIR2111-5* was expressed neither in roots, root nodules, nor stems.**
a-d *L. japonicus* seedlings stably transformed with GUS reporter gene with expression driven by a 3.0 kb DNA fragment upstream of *MIR2111-5* were incubated in GUS staining buffer for 3 h. Roots (a, c), root nodules (7 days after inoculation) (b), and stems (d). Xy: xylem; Ph: phloem.

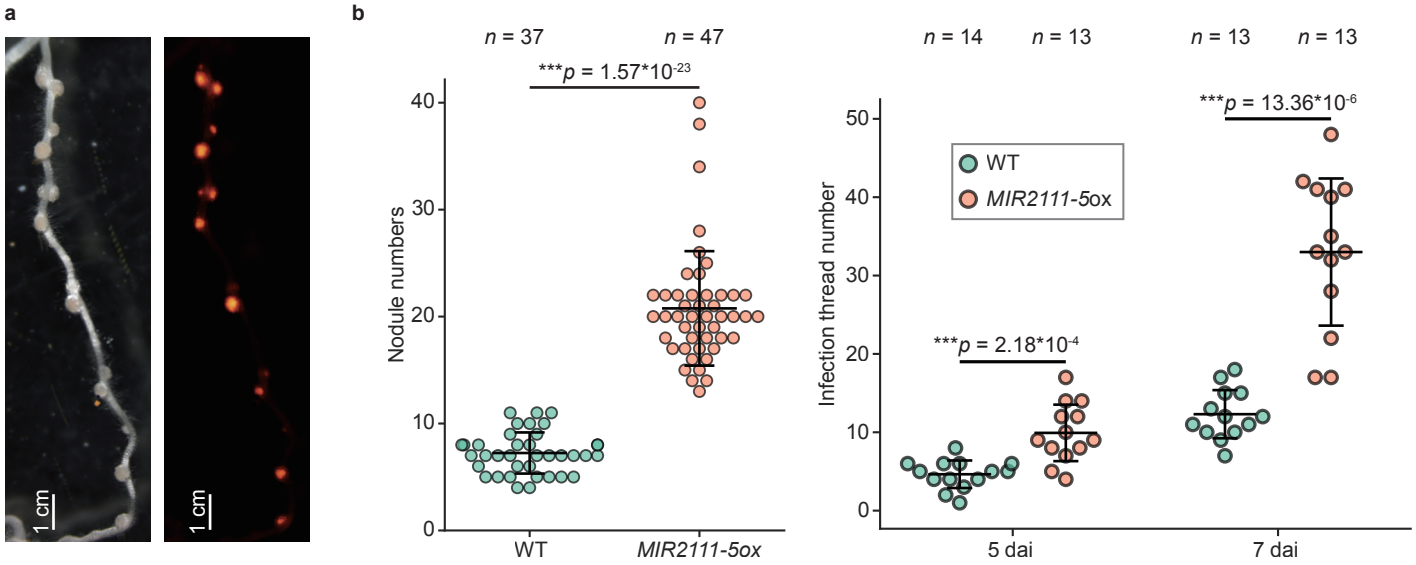

Figure 2.7: Over-expression of *MIR2111-5* induced hypernodulation and accumulation of mature miR2111s.

Figure 2.7: Overexpression of *MIR2111-5* induced hypernodulation and accumulation of mature miR2111s.

a Nodulation on *MIR2111-5*ox (21 days after inoculation). A bright image (*Left*) and corresponding fluorescence image of DsRed expressing in *M. loti* (*Right*). **b** Number of nodules (21 days after inoculation) and infection threads (5 and 7 days after inoculation) formed in wild-type and *MIR2111-5*ox roots. Scatterplots show individual biological replicates as dots. Bars indicate mean ± standard deviation. Two-sided Student's *t*-test was used to determine statistical difference compared with wild-type plants: ***, $p < 0.001$.

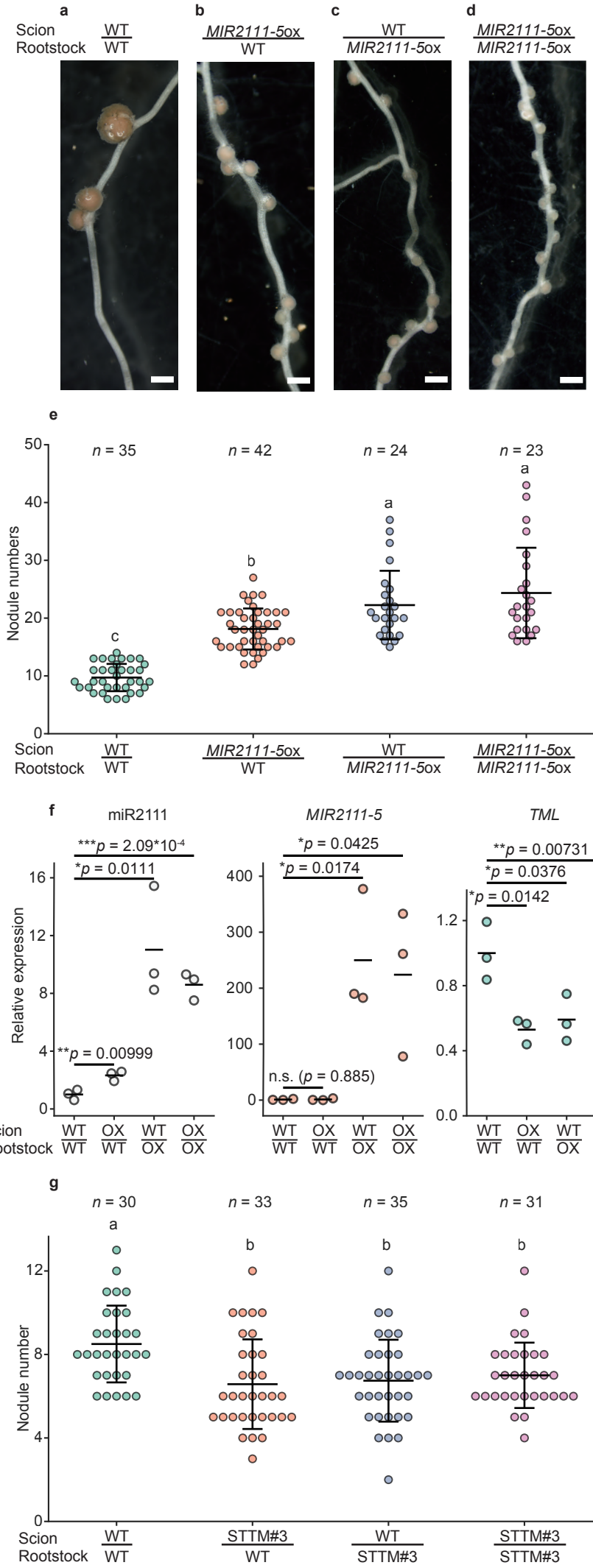

Figure 2.8: Reciprocal grafting between wild-type and either *MIR2111-5* over-expression or STTM2111 plants.

Figure 2.8: Reciprocal grafting between wild-type and either *MIR2111-5* overexpression or STTM2111 plants.

a-e Nodulation at 28 days after inoculation (dai) in wild-type (a,b) and *MIR2111-5*ox (c,d) rootstocks grafted with wild-type (a,c) and *MIR2111-5*ox (b,d) scions. Scale bars: 1 mm. **e** Nodule numbers on rootstocks of grafted plants (28 dai). **f** qRT-PCR analyses of mature miR2111s, *MIR2111-5*, and *TML* in rootstocks of the grafted plants (5 dai). OX represents *MIR2111-5*ox plants. All values were normalized by the mean value of wild-type self-grafting plants. $n = 3$ individual biological replicates for each treatment. Bars indicate mean values. Two-sided Student's *t*-test was used to determine statistical difference compared with wild-type self-grafting plants: *, $p < 0.05$; **, $p < 0.01$; ***, $p < 0.001$; n.s., not significant. **g** Nodule numbers in rootstocks of grafted plants between WT and STTM2111 (21 dai). STTM represents STTM2111 plants. (e-g) Scatterplots show individual biological replicates as dots. Different letters indicate significant differences ($p < 0.05$) from Tukey's honestly significant difference test. (e, g) Bars indicate mean ± standard deviation.

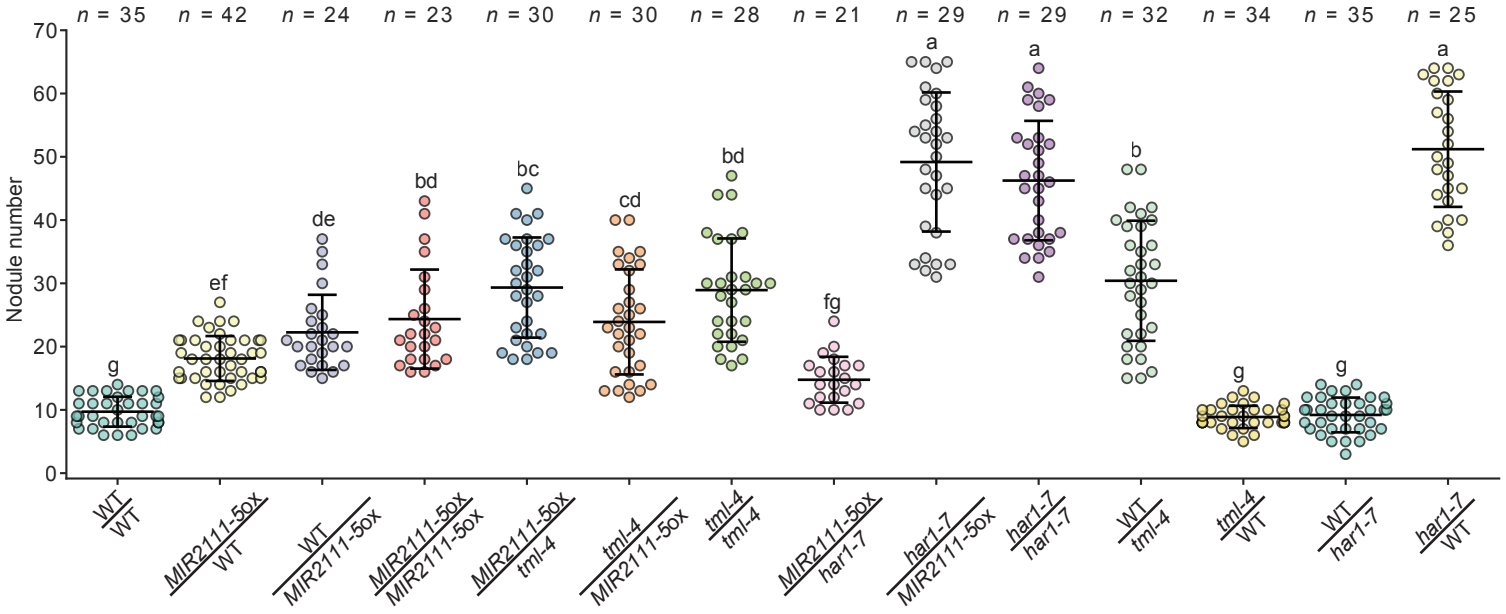

Figure 2.9: Reciprocal grafting of wild-type, *har1-7*, *tml-4*, and *MIR2111-5*ox.

Figure 2.9: Reciprocal grafting of wild-type, *har1-7*, *tml-4*, and *MIR2111-5*ox.
Numbers of nodules (28 days after inoculation) formed in rootstocks of reciprocal and self grafted plants. Scatterplots show individual biological replicates as dots. Bars indicate mean ± standard deviation. Different letters indicate significant differences ($p < 0.05$) from Tukey's honestly significant difference test.

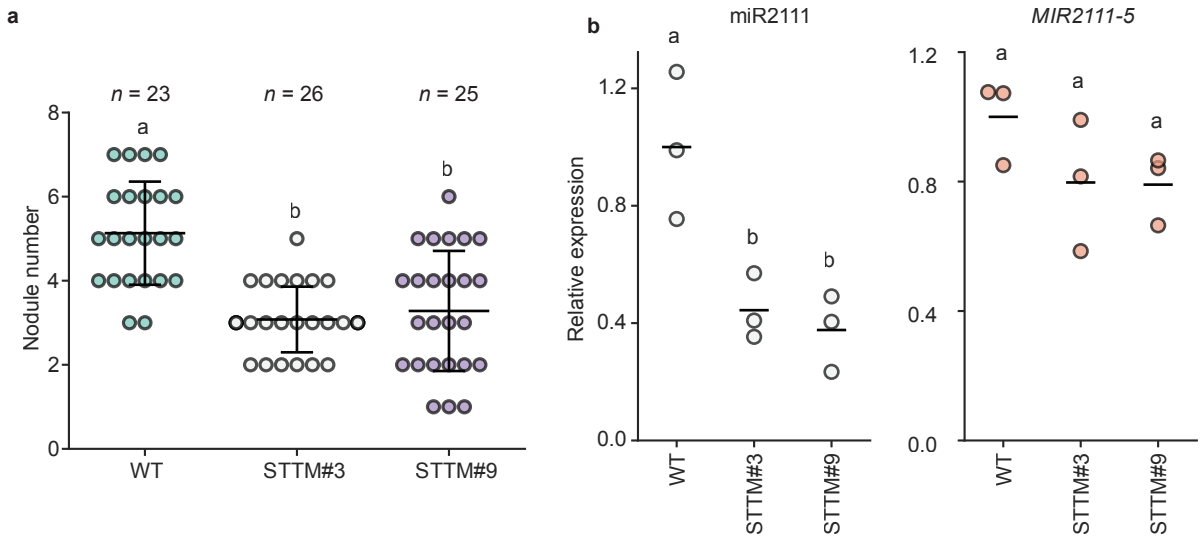

Figure 2.10: STTM2111 plants showed significant decrease in nodule numbers and mature miR2111s levels.

Figure 2.10: STTM2111 plants showed significant decrease in nodule numbers and mature miR2111s levels.

a Nodule numbers on wild-type and stable transformed lines of STTM2111 (21 days after inoculation). Bars indicate mean ± standard deviation. **b** qRT-PCR analyses of mature miR2111s and *MIR2111-5* in leaves of wild-type and STTM2111 lines. $n = 3$ individual biological replicates for each treatment. Bars indicate mean values. (a, b) STTM represents STTM2111 plants. Scatterplots show individual biological replicates as dots. Different letters indicate significant differences ($p < 0.05$) from Tukey's honestly significant difference test.

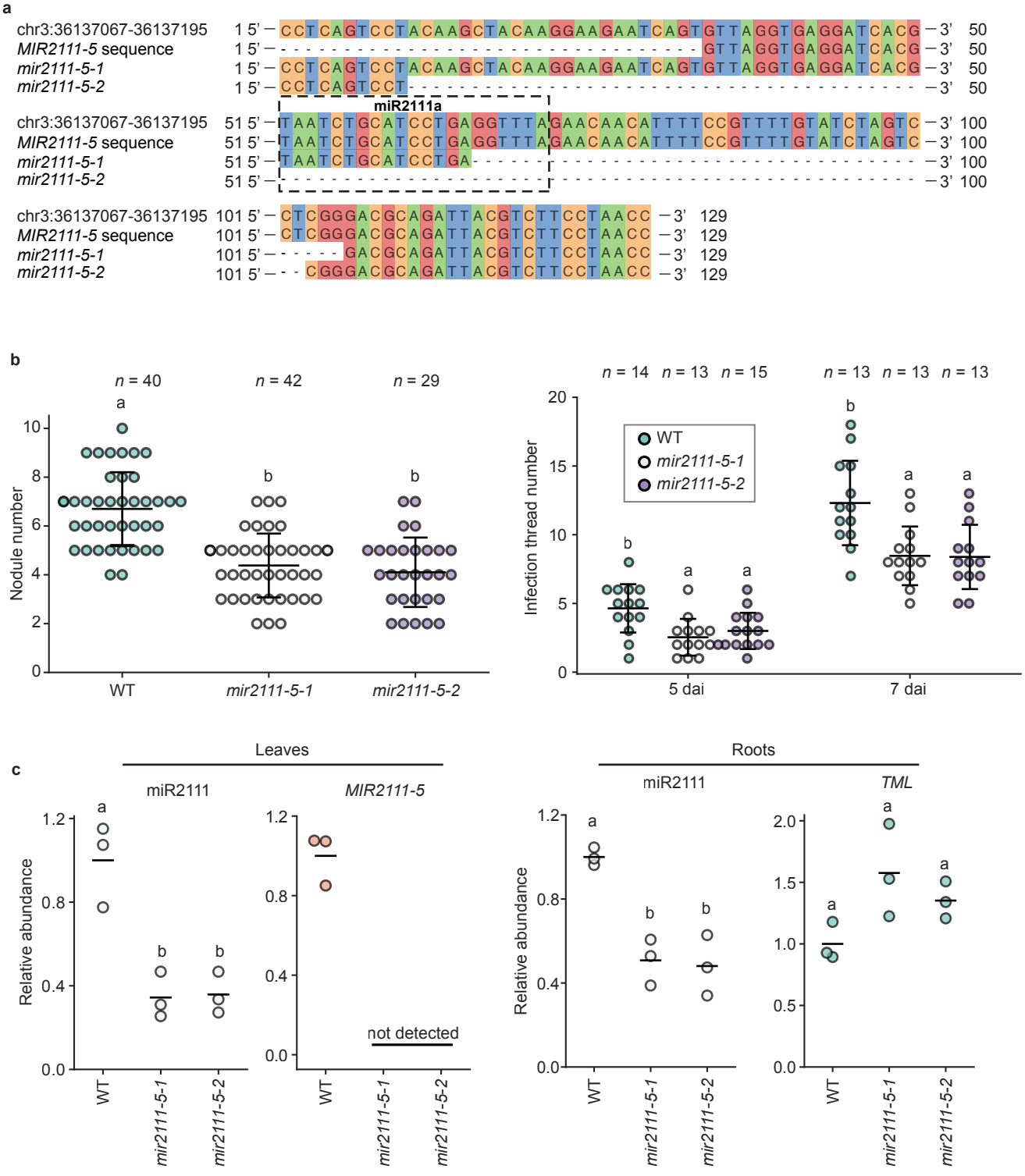

Figure 2.11: *MIR2111-5* knockout significantly inhibited nodulation and accumulation of mature miR2111s.

Figure 2.11: *MIR2111-5* knockout significantly inhibited nodulation and accumulation of mature miR2111s.

a Nucleotide sequences of *MIR2111-5* and its knockout lines. **b** Numbers of nodules (21 days after inoculation) and infection threads (5 and 7 days after inoculation) roots of wild-type, *mir2111-5-1*, and *mir2111-5-2* (21 days after inoculation). Bars indicate mean ± standard deviation. **c** qRT-PCR analyses of mature miR2111s, *MIR2111-5*, and *TML* in leaves and roots at 14 and 7 days after germination, respectively. $n = 3$ individual biological replicates for each treatment. Bars indicate mean values. (b, c) Scatterplots show individual biological replicates as dots. Different letters indicate significant differences ($p < 0.05$) from Tukey's honestly significant difference test.

Table 2.1: List of miR2111 genes, miR2111 hairpin sequences, and mature miR2111s.

miR2111 genes and corresponding miR2111 hairpin sequences and mature miR2111s are shown in table. The position and length columns refer to chromosomal positions and nucleotide sequence lengths of miR2111 genes and hairpin sequences, respectively.

miR2111 gene	Position (Gene)	Length (bp) (Gene)	Mature miR2111	Direction of mature miR2111	miR2111 hairpin sequence name	Position (Hairpin sequence)	Length (bp) (Hairpin sequence)	Reference
MIR2111-1	chr1:111758592-111758787	196	miR2111a	+	miR2111-A	chr1:111758703-111758787	85	Tsikou *et al* ., 2018
MIR2111-2	chr3:34123742-34124530	789	miR2111b	+	miR2111-B	chr3:34123776-34123853	78	Tsikou *et al* ., 2018
			miR2111c	+	miR2111-C	chr3:34123929-34124029	101	Tsikou *et al* ., 2018
MIR2111-3	chr3:36146068-36145746	323	miR2111a	-	miR2111-D	chr3:36145845-36145747	99	Tsikou *et al* ., 2018
			miR2111b	-	miR2111-E	chr3:36146011-36145914	98	Tsikou *et al* ., 2018
MIR2111-4	chr3:34163935-34164541	607	miR2111a	+	miR2111-F	chr3:34164032-34164099	68	This study
MIR2111-5	chr3:36137160-36136263	898	miR2111a	-	miR2111-G	chr3:36137158-36137067	92	This study
MIR2111-6	chr3:34133426-34134047	622	miR2111a	+	miR2111-H	chr3:34133526-34133595	70	This study
MIR2111-7	chr3:34151024-34151700	677	miR2111b	+	miR2111-I	chr3:34151063-34151140	78	This study
			miR2111c	+	miR2111-J	chr3:34151231-34151294	64	This study

Table 2.2: List of primers, oligonucleotides, and synthesized DNA fragment.

		Forward (5' --> 3')	Reverse (5' --> 3')
Clonining primers	*MIR2111-2*	ATCCGGTACCGAATTTCCATTGGCTCAATACTTGG	GTGCGGCCGCGAATTTCGGTCAAATTGACCAAAGC
	MIR2111-4	ATCCGGTACCGAATTTACAAGGACTCTTCTTATAGA	GTGCGGCCGCGAATTTTCAGGAAACTAGAACACAAA
	MIR2111-5	ATCCGGTACCGAATTGTTAGGTGAGGATCACGTA	GTGCGGCCGCGAATTAGGAAAACAAGGTTTAACCAT
	MIR2111-5 promoter (3 kb)	ATCCGGTACCGAATTGTTAGGGGCTAATCGATTTT	GTGCGGCCGCGAATTACTGATTCTTCCTTGTAGCT
qRT-PCR primers	miR2111	TAATCTGCATCCTGAGGTTTA	
	MIR2111-5	GGTTTAGAACAACATTTTCCG	GTAATCTGCGTCCCGAGGAC
	TML	GCCAACAATTGCCTGAAACCAGATG	CTTTATGGTGTTTCTCTCTATGAATGCTG
	Ubiquitin	ATGCAGATCTTCGTCAAGACCTTG	ACCTCCCCTCAGACGAAG
	ATP synthase	CAATGTCGCCAAGGCCCATGGTG	AACACCACTCTCGATCATTTCTCTG
Oligonucleotides for CRISPR gRNA	*mir2111-5-1A*	ATTGGAAGACGTAATCTGCGTCCCG	AAACCGGGACGCAGATTACGTCTTC
	mir2111-5-1B	ATTGGAAAATGTTGTTCTAAACCTC	AAACGAGGTTTAGAACAACATTTTC
	mir2111-5-2A	ATTGGCCCGAGGACTAGATACAAAA	AAACTTTTGTATCTAGTCCTCGGGC
	mir2111-5-2B	ATTGGCCTTGTAGCTTGTAGGACTG	AAACCAGTCCTACAAGCTACAAGGC
Primers and oligonucleotides for modification of pMR203/PMR285 vector	pMR203_AB	ATTGGGCCCTCTAGAGGATCCCCTAAGGTTGTACAAAAAAGCAGGCTTAC	ATTCTGCAGGGTACCGTCGACCCTAAGGTTTGTATAGAAAAGTTGGGTGC
	pMR203_BC	ATTGGGCCCGGATCCGTCGACCCTTAGGTTGTACAAAAAAGCAGGCTTAC	ATTCTGCAGGGTACCTCTAGACCTGAGGTTTGTATAGAAAAGTTGGGTGC
	pMR285_oligo	ATTGCTGCAGCCTAAGGAAAATCGGCCTGAGGGGATCCAATGCCGTCGA	AAACCTGCAGGGTACCAATCGGTCTAGAGGCATTGTCGACGGCATTGGAT
		CAATGCCTCTAGACCGATTGGTACCCTGCAG	CCCCTCAGGCCGATTTTCCTTAGGCTGCAG
Synthetic STTM miR2111-88 nt spacer with attL1 and attL2 (5' --> 3')		ATAGGGCGAATTGGCGGAAGGCCGTCAAGGCCGCATCAACGAGCTCCAAATAATGATTTTATTTTGACTGATAGTGACC	
		TGTTCGTTGCAACAAATTGATAAGCAATGCTTTTTTATAATGCCAACTTTGTACAAAAAAGCAGGCTTAAACCTCAGGC	

Table 2.3: Summary of RNA-seq reads.

Index name	Description	No. of raw reads	No. of trimmed reads	No. of mapped reads (more than MAPQ = 30)
idx1	WT (MG-20) Mock replicate 1	30,808,995	30,467,270	28,445,920
idx2	WT (MG-20) Mock replicate 2	34,663,575	34,302,126	31,964,562
idx3	WT (MG-20) Mock replicate 3	26,253,097	25,932,116	24,084,516
idx4	WT (MG-20) inoculated replicate 1	30,185,644	29,859,787	27,719,358
idx5	WT (MG-20) inoculated replicate 2	27,191,690	26,905,799	24,975,835
idx6	WT (MG-20) inoculated replicate 3	27,041,726	26,749,774	24,824,295
idx10	har1-7 Mock replicate 1	25,996,589	25,737,531	23,537,190
idx11	har1-7 Mock replicate 2	25,387,350	25,113,274	22,774,526
idx12	har1-7 Mock replicate 3	26,440,567	26,174,251	24,189,348
idx13	har1-7 inoculated replicate 1	25,124,702	24,845,951	23,065,335
idx14	har1-7 inoculated replicate 2	22,991,791	22,749,322	21,146,191
idx15	har1-7 inoculated replicate 3	35,760,799	35,378,641	32,912,653

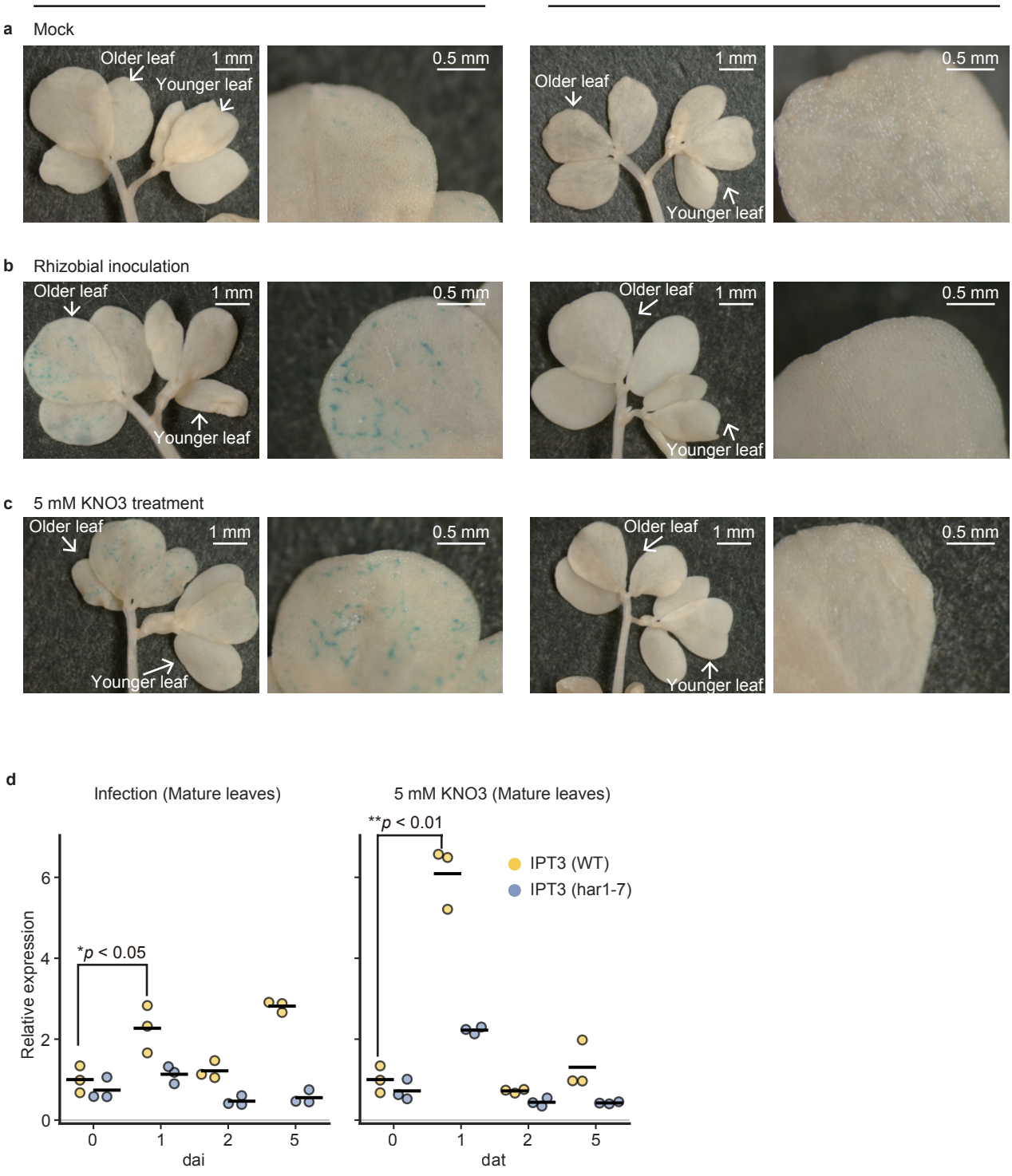

Figure 3.1: *IPT3* was expressed mainly in the vascular bundle of mature leaves in a HAR1-dependent manner.

Figure 3.1: *IPT3* was expressed mainly in the vascular bundle of mature leaves in a HAR1-dependent manner

a-c GUS expression controlled by a 2.0 kb DNA fragment upstream of *IPT3* in true leaves of WT *proIPT3*:GUS and *har1-7 proIPT3*:GUS plants mock-treated (a), inoculated with *M. loti* (1 day after inoculation) (b), and treated with 5 mM KNO_3, were incubated in GUS staining buffer for 18 h. **d** qRT-PCR analyses of *IPT3* in mature leaves at indicated days after either inoculation (dai) with *M. loti* or treated with 5 mM KNO_3. Scatterplots show individual biological replicates as dots. Bars indicate mean values. All values were normalized by the mean value of wild-type mock-treated leaves. Two-sided Student's *t*-test was used to determine statistical difference compared with mock control: *, $p < 0.05$; **, $p < 0.01$.

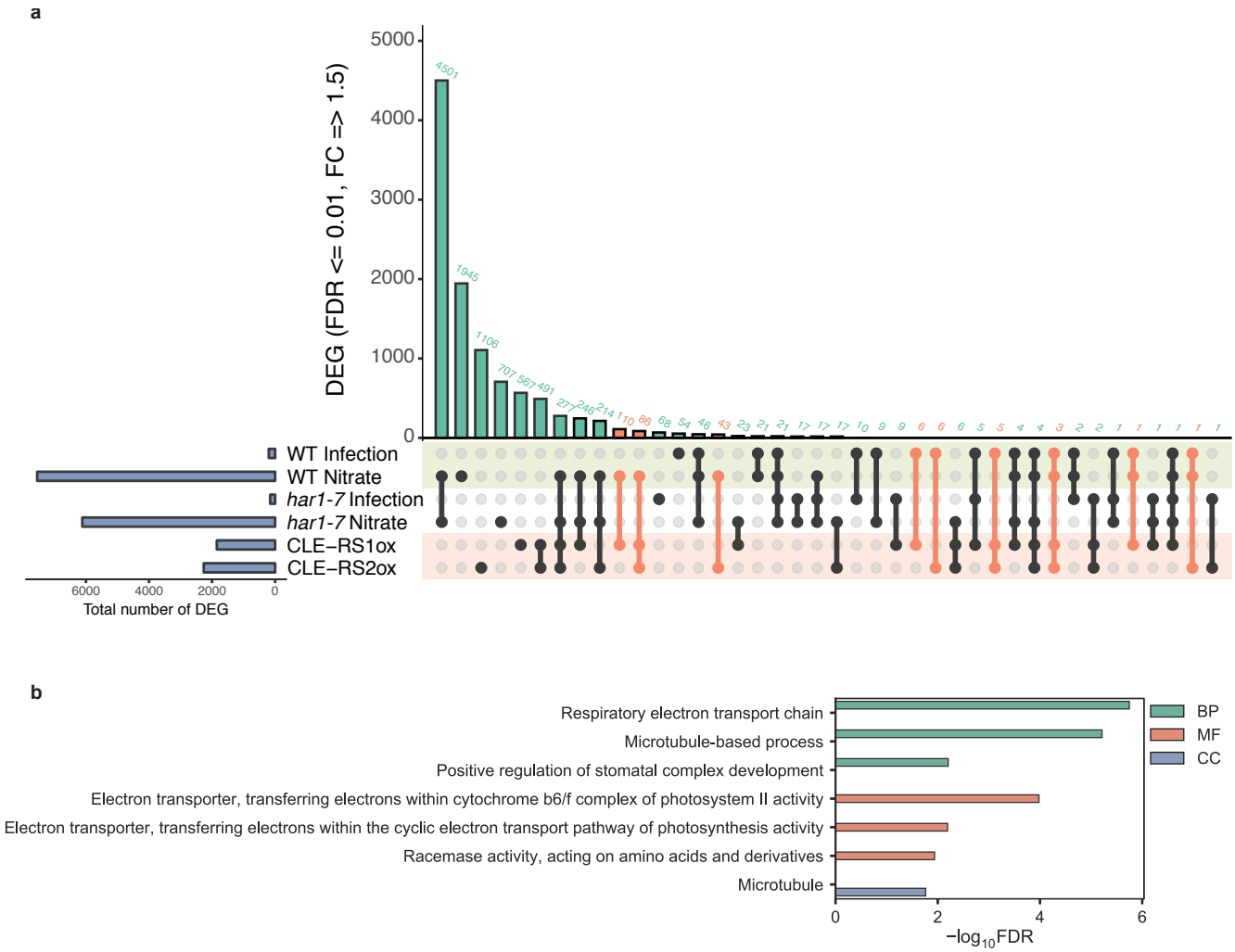

Figure 3.2 RNA-seq analysis of WT, *har1-7*, *CLE-RS1*ox, and *RS2*ox leaves.

Figure 3.2: RNA-seq analysis of WT, *har1-7*, *CLE-RS1*ox, and *CLE-RS2*ox leaves.
a Upset plot delineating the number of upregulated genes in response to the indicated treatments compared with mock treatments. The vertical bar chart indicates the number of upregulated genes that are shared between the treatments indicated by the connection of dots below. The horizontal bar chart indicates the total number of upregulated genes in each treatment. The orange highlights indicate the groups of genes that were commonly upregulated in response to rhizobial inoculation or treatment with 5 mM KNO_3 and *CLE-RS1* or *CLE-RS2* overexpression in a HAR1-dependent manner. DEG: differentially expressed gene; FDR: false discovery rate; FC: fold change
b Results of gene ontology (GO) enrichment analysis for the groups highlighted orange in Fig. 3.2a. BP: biological process; MF: molecular function; CC: cellular component

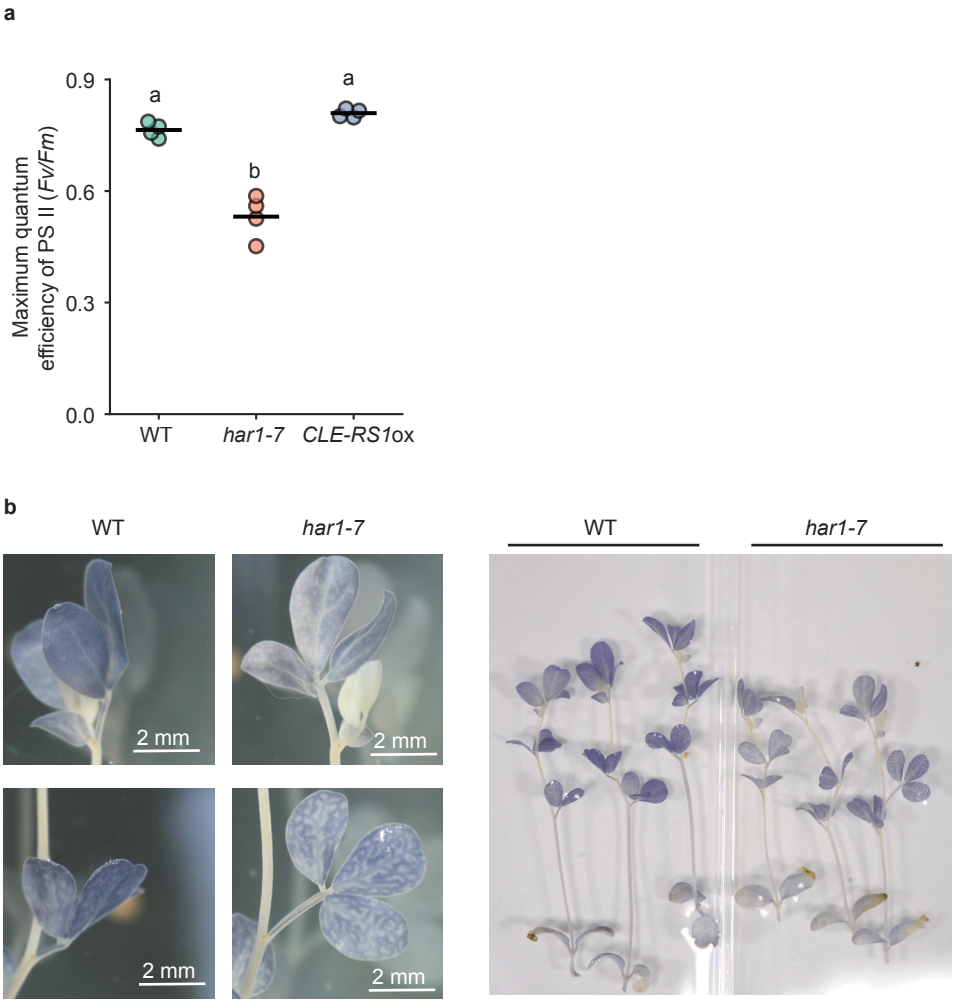

Figure 3.3 Analysis of *Fv/Fm* by PAM and staining of starch by iodine.

Figure 3.3: Analysis of *Fv/Fm* by PAM and staining of starch by iodine.

a *Fv/Fm* of fully expanded leaves of WT, *har1-7*, and *CLE-RS1*ox in one month after germination. $n = 4$ individual biological replicates for each treatment. Bars indicate mean values. Scatterplots show individual biological replicates as dots. Different letters indicate significant differences ($p < 0.05$) from Tukey's honestly significant difference test.

b Starch in shoots stained with iodine

Table 3.1:The list of genes related to photosynthesis or with enriched gene ontology (GO) terms, which were upregulated in response to nitrate treatment depending on HAR1

The list of genes related to photosynthesis or with enriched GO terms, which were upregulated in response to nitrate treatment depending on HAR1.
All genes in this table were extracted with a false discovery rate< 0.01 and fold change > 1.5.

Gene_id	Annotation	BLAST best hit in A. thaliana
Ljchlorog3v0000170	YCF3-like (PSI assembly protein)	ATCG00360.1;photosystem_I_assembly_protein
Ljchlorog3v0010750	PSBH-like (Photosystem II protein H)	ATCG00710.1;photosystem_II_reaction_center_protein_H
Ljchlorog3v0010730	PSBB-like (Photosystem II 47 kDa protein)	ATCG00680.1;photosystem_II_reaction_center_protein_B
Ljchlorog3v0010800	PETD-like (Cytochrome b6/f complex subunit IV)	ATCG00730.1;photosynthetic_electron_transfer_D
Ljchlorog3v0010770	PETB partial (cytochrome b(6) subunit of the cytochrome b6f complex)	ATCG00720.1;photosynthetic_electron_transfer_B
Lj0g3v0160269	PETB partial (cytochrome b(6) subunit of the cytochrome b6f complex)	ATCG00720.1;photosynthetic_electron_transfer_B
Lj0g3v0309079	Cytochrome b-like	AT2G07727.1;cytochrome_b
Lj1g3v3593870	Stomagen-like	AT4G12970.1;stomagen
Lj0g3v0149239	Sec61-beta subunit protein-like	AT2G45070.3;Preprotein_translocase_Sec%2C_Sec61-beta_subunit_protein
Lj0g3v0267899	Tubulin/FtsZ family protein	AT4G14960.1;Tubulin/FtsZ_family_protein
Lj0g3v0267939	Tubulin/FtsZ family protein	AT4G14960.2;Tubulin/FtsZ_family_protein
Lj0g3v0267879	Tubulin/FtsZ family protein	AT4G14960.1;Tubulin/FtsZ_family_protein
Lj0g3v0267859	Tubulin alpha-5 like	AT5G19780.1;tubulin_alpha-5
Lj1g3v2095980	Tubulin alpha-7 chain-like	AT4G14960.2;Tubulin/FtsZ_family_protein
Lj5g3v2065190	Tubulin alpha chain-like	AT1G50010.1;tubulin_alpha-2_chain
Lj6g3v0802330	Kinesin-like protein KIN12B-like isoform X1	AT3G20150.2;Kinesin_motor_family_protein
Lj0g3v0131319	Protein transport protein Sec61 subunit beta-like isoform 1	AT2G45070.1;Preprotein_translocase_Sec%2C_Sec61-beta_subunit_protein
Lj3g3v0075760	Probable amino-acid racemase-like	AT1G15410.1;aspartate-glutamate_racemase_family
Lj3g3v2224710	Probable amino-acid racemase-like	AT1G15410.1;aspartate-glutamate_racemase_family